Diagenesis and Petrographic Characterization of Surma Group Sandstone in the South-Eastern Part of Bangladesh: Implications for Reservoir Quality Assessment

Mohammad Saiful Islam[1,2], Xiwu Luan[2], Tamanna Meheran Shemu[1], Zohur Ahmed[1], Md. Anwar Hossain Bhuiyan[1] and Mohammad Solaiman[1]*

[1]Department of Geology, University of Dhaka, Dhaka-1000, Bangladesh
[2]College of Earth Science and Engineering, Shandong University of Science and Technology, Qingdao 266590, China

Manuscript received: 25 February 2026; accepted for publication: 16 July 2026

ABSTRACT: The Neogene Surma Group sandstones exposed in the Sitapahar (Kaptai) and Sitakund structures of the Eastern Fold Belt, Bengal Basin, constitute important hydrocarbon-potential reservoirs whose quality is strongly influenced by depositional architecture and diagenetic evolution. This study integrates outcrop sedimentology, petrography, Field-Emission Scanning Electron Microscopy (FE-SEM), and Energy-Dispersive Spectroscopy (EDS) to evaluate lithofacies distribution, diagenetic alterations, and reservoir quality controls within these sandstones. Detailed facies analysis identified depositional associations related to delta front-shoreface, delta plain, tidal flat, prodeltaic, tidal-influenced channel-fill, and channel-bypass systems, indicating deposition within a tide-dominated deltaic-shallow-marine environment. Petrographic analyses reveal predominantly medium- to fine-grained, moderately to well-sorted sublitharenites composed mainly of quartz with subordinate lithic fragments and feldspars, reflecting moderate compositional maturity. Thin-section porosity ranges from 5–23%, with generally low matrix content (<4%). Diagenetic processes, including mechanical compaction, pressure solution, quartz overgrowth, calcite cementation, chlorite coating, and clay mineral authigenesis, significantly modified the primary pore framework and reduced reservoir quality. Conversely, dissolution of feldspar, lithic fragments, and carbonate cements generated secondary porosity and enhanced pore connectivity. FE-SEM observations confirm the presence of interconnected intergranular and intragranular pore systems, although pore-throat reduction by chlorite and illite-smectite coatings locally restricted permeability. Comparative analyses indicate better reservoir quality in the Sitapahar sandstones than in the Sitakund deposits, due to differences in depositional texture and diagenetic intensity. Overall, the Surma Group sandstones exhibit promising reservoir characteristics with significant implications for hydrocarbon exploration in the Eastern Fold Belt of Bangladesh.

Keywords: Surma Group; Sandstone Diagenesis; Petrography; Reservoir Quality; Porosity-Permeability; Bengal Basin

INTRODUCTION

The Eastern Fold Belt, also known as the Frontal Fold Belt, is the most prolific hydrocarbon province in Bangladesh (Khan & Chouhan, 1996; Uddin & Lundberg, 2004). This tectonically active belt hosts 29 gas fields, primarily occurring at depths of approximately 1,000–3,000 m (Imam, 2013; BAPEX, 2020). Within this framework, the Surma Group, comprising the Miocene Bhuban and Bokabil formations, forms one of the most extensive clastic successions in the Bengal Basin and constitutes a major hydrocarbon-bearing interval in the south-eastern fold belt (Reimann, 1993). Given the economic importance of these Miocene reservoirs, a detailed understanding of their petrographic characteristics and diagenetic evolution is essential for reliable reservoir quality assessment.

Reservoir quality within the Surma Group sandstones is highly variable and is strongly influenced by diagenetic processes associated with burial and post-burial fluid evolution (Islam, 2009; Rahman & McCann, 2012; Rahman & Worden, 2016; Rahman et al., 2022; Sayem et al., 2022; Akter et al., 2023; Paul et al., 2025). Although depositional attributes such as grain size, sorting, and sedimentary facies exert primary control on initial porosity and permeability, burial diagenesis commonly overprints these characteristics and exerts a dominant control on reservoir quality. Previous studies indicate that mechanical compaction, quartz overgrowth, carbonate cementation, feldspar alteration, and the precipitation of authigenic clay minerals (e.g., kaolinite, chlorite, and illite) significantly reduce pore volume and pore-throat connectivity in Bengal

Corresponding Author: Mohammad Solaiman
Email: solaiman@du.ac.bd

DOI: https://doi.org/10.3329/dujees.v15i1.92368

Basin sandstones (Bashar & Khan, 2008; Islam & Habibullah, 2017). Quartz and carbonate cements are widely recognized as major porosity-reducing agents, whereas dissolution of feldspar and lithic fragments may enhance secondary porosity in certain intervals (Imam & Shaw, 1985; Chowdhury & Samanta, 2004). Comparable diagenetic trends have been reported from other foreland basin systems, where rapid sedimentation and evolving pore-fluid chemistry contribute to pronounced diagenetic heterogeneity (Morad et al., 2000; Worden & Burley, 2003).

Despite these advances, the integrated influence of depositional conditions and diagenetic processes on reservoir quality in the Surma Group sandstones of the Eastern Fold Belt remains insufficiently constrained, particularly in the south-eastern fold belt. To address this gap, the present study focuses on two structurally significant and comparatively less investigated areas - Kaptai (Rangamati) and Sitakund (Chattogram), within the south-eastern Bengal Basin. These locations were selected because they provide well-exposed outcrops of Surma Group sandstones within distinct structural settings, allowing direct comparison of depositional and diagenetic controls on reservoir quality. The study specifically examines the Sitapahar structure in Kaptai, a symmetrical box-type anticline, and the Sitakund structure, a doubly plunging, asymmetric anticline. Both structures belong to the NNW–SSE-trending Chittagong–Tripura Fold Belt, where anticline axes are aligned parallel to the regional hill ranges.

This study documents lithofacies associations and interprets depositional environments through systematic outcrop logging of stratigraphic sections in these areas, while also characterizing the textural and compositional attributes of the sandstones using detailed petrographic analysis. Diagenetic features, pore types, and mineralogical alterations are further investigated using Field-Emission Scanning Electron Microscopy (FE-SEM) and Energy-Dispersive Spectroscopy (EDS). The study ultimately evaluates how the interplay between depositional controls and diagenetic evolution governs reservoir quality, with particular emphasis on porosity, pore-throat characteristics, and reservoir heterogeneity. This integrated approach provides a process-based framework for understanding spatial variations in reservoir properties within these economically significant Miocene sandstones.

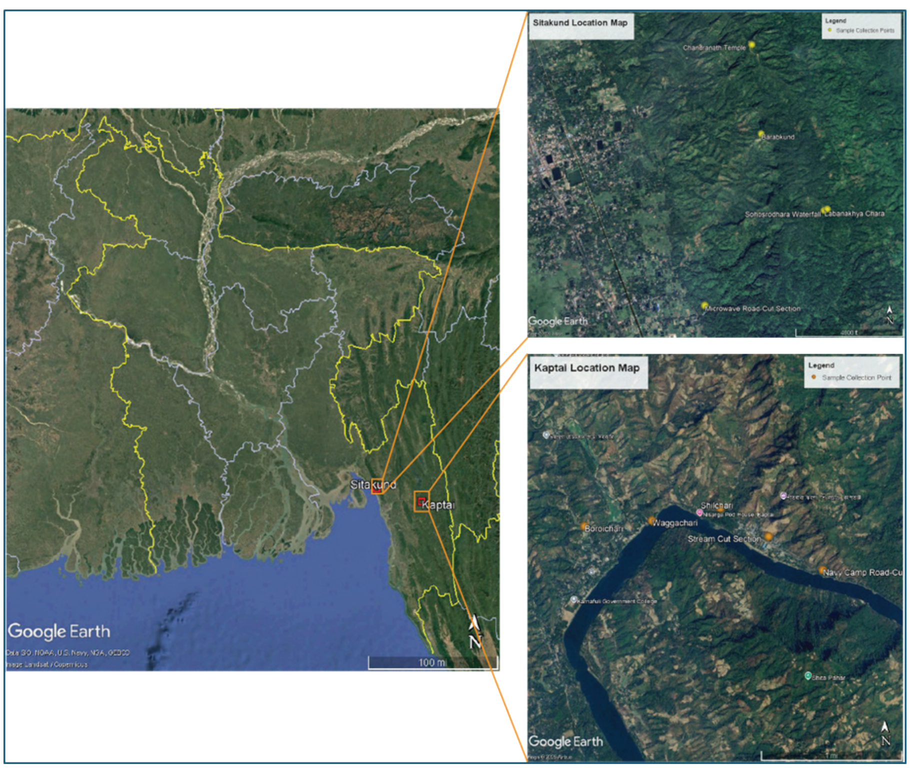

Figure 1: Study Area Shown in a Geographic Map of Bangladesh (Left). The Google Earth Image is the Primary Source of the Map. The Outcrop Locations are Shown in the Sitakund Area (upper right) and the Kaptai Area (lower right)

GEOLOGICAL SETTING

Regional Tectonic Setting

The Bengal Basin originated from the collision of the Eurasian and Burmese plates (Alam et al., 2003). The Bengal Basin was formed in part by the Himalayan orogeny and the closure of the Tethys Sea. The Indo-Burman ranges were created during the Eocene-Oligocene time by the uplift of the accretionary prism that resulted from the collision of the Indian and Burmese plates (Curray & Moore, 1974). The basin is bordered by the Indo-Burman Range to the east, the Indian shield in the west, and the Himalayan and Shillong massif to the north. The basin is open towards the Bay of Bengal. The formation of the basin was initiated due to the breakup of Gondwana during the late Cretaceous, a process that is still ongoing (Alam, 1989). Here, a sedimentary succession of about 22 km is recorded over the time interval from the Early Cretaceous to the Holocene. Shallow marine to continental clastic sedimentary rocks, with minor carbonates, are predominantly observed here (Alam et al., 2003). During the Miocene, this basin began to receive a substantial volume of clastic sediments from the Ganges-Brahmaputra and ancestral rivers from the Himalayan and Indo-Burman ranges (Uddin & Lundberg, 1999). The Bengal basin is around 500 km wide in the south and 200 km wide in the north (Hossain et al., 2019).

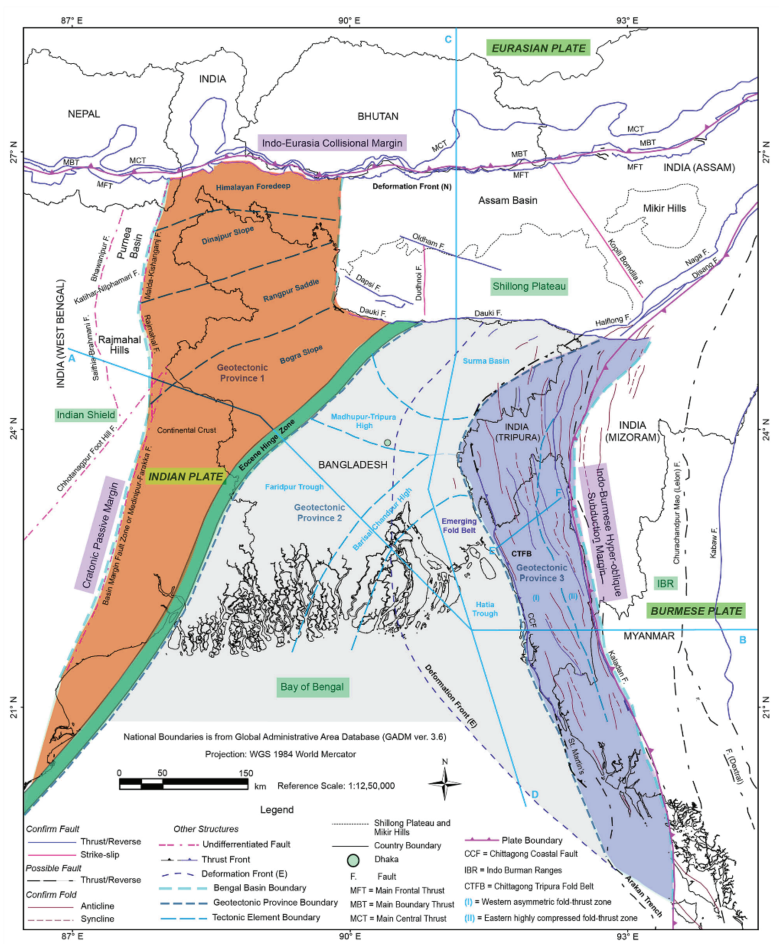

Figure 2: Bangladesh and its Major Structural Elements and Regional Tectonic Setting (Modified after Hossain et al., 2020)

The eastern fold belt is considered the western portion of the Indo-Burman Ranges (Hiller, 1988; Johnson & Alam, 1991; Lohmann, 1995). The deep basinal part of the Bengal Basin borders the fold belt on the west, while the thrust sheets of the Indo-Burman fold systems border it on the east. The eastern fold belt contains a thick succession of clastic rocks, including sandstone, shale, and sandy shale, primarily comprising the Neogene sedimentary succession. This sedimentary sequence has experienced less deformation than the sequences in the Indo-Burman fold ranges in the east. The fold belt commonly shows north-south trending, elongated anticlines and synclines (Sikder 1998).

The sedimentation pattern of the basin is primarily controlled by the Ganges-Brahmaputra Delta and its extensive river system (Goodbred & Kuehl, 2000; Allison et al., 2003). Compared to the pre-Miocene units of the Bengal Basin and the western Himalayan foreland basins, the sand deposits in this basin are typically less lithic and more quartzose. (Uddin & Lundberg, 1998; Najman et al., 2008). This compositional contrast reflects the influence of orogenic activity on sediment supply, suggesting that the sedimentary system migrated southward in response to the progressive eastward advancement of the mountain belt and the closure of the remnant ocean (Johnson & Alam, 1991; Uddin & Lundberg, 1998). Ongoing orogenic uplift, coupled with subsidence within the basin, facilitated the accumulation of alternating arenaceous and argillaceous clastic successions that constitute the Surma Group across the broader basin, including the Surma Valley, Tripura, and the Chittagong Hill Tracts (Reimann, 1993; Alam et al., 2003). These alternating facies reflect a complex interplay of deltaic sub-environments, punctuated by minor marine incursions associated with episodes of significant marine regression and intermittent transgression (Banerjee & Sen, 1988; Alam et al., 2003) (Fig. 2).

Stratigraphic Succession

The study areas lie within the Chittagong-Tripura Fold Belt, a former geosynclinal region that later underwent significant folding due to continued tectonic compression associated with the Indo-Burma plate interaction (Reimann, 1993; Uddin & Lundberg, 1998; Alam et al., 2003).

Our study areas are in the Chittagong Tripura Fold Belt, so a general stratigraphy of this specific region is provided in Table 1. It is similar to the generalized stratigraphy of the Bengal Basin, as it is part of a geosynclinal area that later folded due to tectonic compression. Here, recent alluvium is at the top of the Plio-Pleistocene-age Dupi Tila. The Tipam group of Pliocene age is overlain by the Dupi Tila and Underlain by the Miocene Surma Group. The Late Oligocene may comprise the base of Bhuban, which is not exposed, and the Barail group of Oligocene age is entirely subsurface (Table 1).

The Surma group was initially named 'Surma series' after the type area, Surma Valley in Assam, by Evans (1932). In the Bengal Basin, the Surma group comprises a thick sedimentary sequence of Miocene-Pliocene age, divided into the upper Boka Bil Formation and the Lower Bhuban Formation (Holtrop & Keizer, 1970). The Bhuban Formation was deposited in various environments, ranging from shallow marine to lower deltaic plain. On the other hand, the Boka Bil Formation was deposited in multiple environments, ranging from marine at the bottom to transitional marine at the top.

Table 1: Stratigraphy of the CTFB (modified after Gani & Alam, 2003)

<table>
<tr><th colspan="2">Age</th><th>Group</th><th>Formation</th><th>Thickness (m)</th><th>Description</th></tr>
<tr><td rowspan="2">Quaternary</td><td>Recent</td><td>Alluvium</td><td>Alluvium</td><td>Variable</td><td></td></tr>
<tr><td>Plio-Pleistocene</td><td>Dupi Tila</td><td>Dupi Tila</td><td rowspan="3">1100-1600</td><td rowspan="3">Yellowish-brown, with a very coarse to fine sand texture.
A gradation from a large-scale, low-sinuosity braided deposits to high-sinuosity meandering deposits. Very high sand shale ratio.</td></tr>
<tr><td rowspan="2"></td><td rowspan="2">Pliocene</td><td rowspan="2">Tipam</td><td>Girujan clay</td></tr>
<tr><td>Tipam Sandstone</td></tr>
</table>

Neogene	Miocene	Surma (Base not exposed)	Boka Bil	1200-1600	Alternating nearshore sand and shelfal mud with regional erosion surfaces. Predominant tidal structures and high sand-shale ratio.
			Bhuban	1000-1500	Predominant slope mud, sandy deposits between the base of the slope
					Turbidites to nearshore tidal sands. No major erosion surfaces.
Paleogene	Oligocene	Barail Group (in subsurface)		2000+	Speculated submarine fan complex within a trench setting and mud-dominated.

Note: Broken lines indicate unconformity

METHODOLOGY

Field Investigations

Fieldwork was conducted in the Boroichari, Wagga, Shilchari, and Navy Camp Road cut and stream cut sections of the Kaptai area, as well as the Chandranath temple section, microwave road section, Labanakhya chara-Sohosrodhara waterfall section, and Barabkund sections of the Sitakund area, as the Surma Group. sandstones are exposed here. Correct sampling and structural and stratigraphic data were collected to better understand the work from different perspectives.

Sedimentological logs were drawn according to field data, which are shown in the Results and Discussion section. Each sample was assigned a number according to the station number, which can be used to identify its location. A total of fourteen samples were chosen for the thin-section petrographic investigation.

Data Analysis

The collected samples were impregnated before thin-section preparation. The impregnated slabs were trimmed and polished with 400- and 600-grade carborundum powders to achieve a smooth surface. Finally, samples were stained with Alizarin Red S, covered with a slip using Canada balsam, cleaned with acetone, and labelled.

Research Petrographic Microscope (LEICA) model DM750P was used for detailed qualitative and quantitative analysis. The modal composition, mineralogy, and porosity of the sandstones were determined using the point counter method, where to quantify the porosity, 300-500 points were traversed per thin section, and the total porosity was calculated as the ratio of the points landing on the pore spaces relative to the total number of points counted.

Field Emission Scanning Electron Microscope (FE-SEM) and Energy Dispersive X-ray Spectrometer (EDS) analysis was conducted at Bangladesh University of Engineering and Technology (BUET), Department of Nanomaterials & Ceramic Engineering, using a JEOL JSM-7600F with a backscattered electron detector.

RESULTS AND DISCUSSION

Based on the field investigation results, 22 facies were identified. The facies with corresponding descriptions and depicted depositional environments are given in Table 2.

Table 2: Identified Lithofacies in the Study Area with Descriptions and Corresponding Depositional Environments

Lithofacies	Description of the lithofacies	Depositional Environment
Channel lag deposit	Coarse, poorly sorted bedload unit including clay gall, pebbles, and coarser-grained sediments at the base.	Tidal/Fluvial channel deposits
Massive bedded sandstone	Fine to medium-grained sandstone, varies in color, and doesn't have any particular structure. Contain pebble, cobble, and other carbonaceous material	Fluvial Channel
Parallel bedded sandstone	Fine to medium-grained sandstones and internally show parallel laminated sandstones.	Upper flow regime deposits (Tidal flat deposits)
Planar cross-bedded sandstone	Medium to fine-grained sandstone, yellowish brown in color, with planar cross bedding	Tidal ridge and tidal channel deposits.
Ripple Cross-bedded sandstone	Fine to medium grained, brownish grey in color with herringbone cross-stratification.	Subtidal deposits.
Trough cross-bedding	Medium to coarse grained, moderately sorted.	Broad and shallow subtidal environment
Cross-laminated sandstone	Fine to medium-grained sandstone with distinct inclined lamination	Distributary fluvial environment
Flame structure	Contain ripple laminated sandstone with flame structures in it.	Tidal flat deposits.
Laminated to thinly bedded sandstone	Fine-grained sandstones with sharp, planar bedding planes.	Delta front/Upper shoreface
Lenticular bedded sandstone	Yellowish brown to grey in color, they contain thin, flat sand lenses (connected or isolated). Contain increased shale content.	Supratidal to intertidal deposits
Parallel laminated sandstone	Fine to medium-grained sandstone with planar laminae, with occasional mica flakes	Upper shoreface deposits
Ripple laminated sandstone	Fine to medium grained, well sorted, grey to light brownish grey in color	Tidal flats, fluvial sediments, shallow marine channels, and submarine fans with turbidity current deposits.
Wavy bedding	Identified by alternating straight to slightly wavy alternation of bluish grey shale and grey colored silty sandstone.	Intertidal deposits
Current ripple siltstone	Unidirectional climbing ripple marks within silt-sized sediments.	Prodeltaic/Distal Bar deposits

Shale with silt streak	Dark grey mudstones with thin, discontinuous silt streaks	Offshore/shelf environment
Fissile shale	Black to dark grey colored shale with fissility.	Shallow marine to shelf deposits
Mudstone or Claystone	Bluish grey, very fine-grained massive mudstone. Occasional silt streaks were found. It lacks internal sedimentary structures except for minor lamination.	Tide-dominated deposits
Nodular Shale	Dark grey in color, very fine-grained with occasional siltstone.	Shallow marine deposits
Flaser bedding	Light grey to brownish grey color, fine to medium grained. Contain increased sand content.	Subtidal to intertidal deposits

The identified facies were stacked to determine the facies associations occurring in the study area, which are described below.

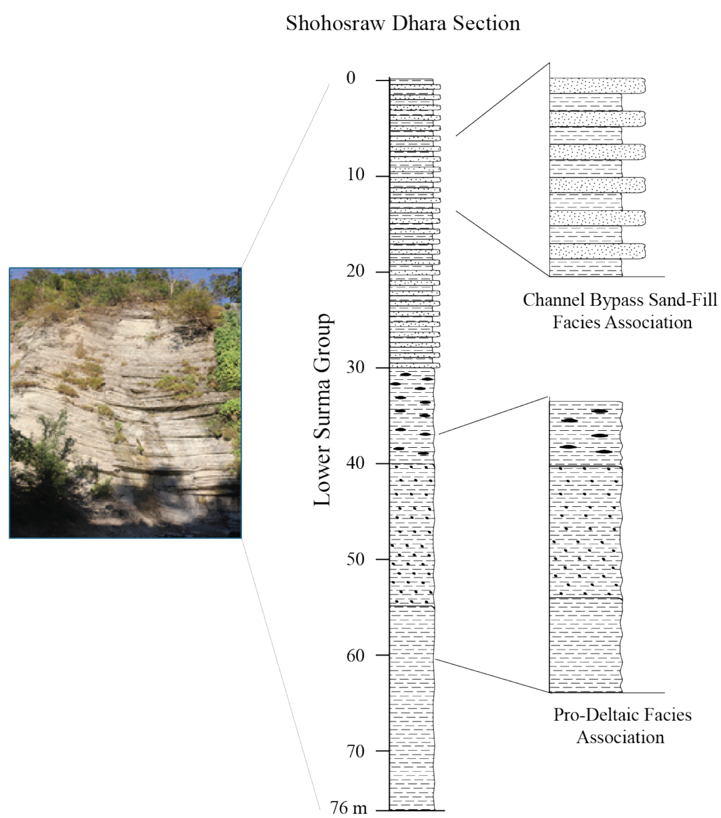

Figure 3: Lithologic Column of the Labanakhya Chara-Sohosrodhara Waterfall Section, Sitakund, Representing Facies Associations

Delta Front Shore Face Facies Association

The regressive facies assemblage, exhibiting massive accumulation of sandstone over prodeltaic shales and heterolithic beds in the study area, reflects a progradational depositional trend with significant aggradation, indicating high-stand system-tract deposits, coarsening upward. This trend suggests that sediment supply outpaced the rise in base level, influenced by upliftment in the source area (Fig. 3).

The regressive facies assemblage comprises heterolithic beds and shale underlie a sandstone unit, approximately 55 meters thick, exhibiting

alternations of sand and shale (Fig. 4). An important characteristic of this sandstone unit is the parallel laminated sandstone and ripple lamination, which indicate a high-energy environmental condition. The delta front shoreface association, crucial in this study, reveals conventional sandstone reservoirs that are discernible from surface exposures.

Delta Plain Facies Association

Within the overall coarsening-upward units of tide-dominated deposits, the facies association is an intriguing mix that includes individual cycles exhibiting a fining-upward sequence. This facies association begins with a basal shale lithology, although with lateral alterations. A series of sandy lithologies increasingly enrich it, culminating in an erosional surface. The sand-dominated facies, a distinctive feature, develops stratigraphic traps of both conventional and unconventional nature in this facies association. The shaly base with a coarsening-upward trend indicates an early highstand normal regression event above the maximum flooding surface, attributed to base-level fall driven by excessive sediment supply from the source area (Figs. 3, 4, and 5).

Tidal Flat Facies Association

Heterolithic beds, such as flaser, wavy, and lenticular bedding deposits, with intermittent laminated to thinly bedded sandstone, make up the majority of this facies association. The Surma Group is well exposed for this facies association in the Labanakkhya Chara Section, Shohosraw Dhara Section, Chandranath Temple Section, Shilchari Section, and Kaptai Road Cut Section. Tidal flat deposits are characterized by fluctuating energy conditions in the intertidal and supratidal deltaic depositional environment. Thin-bed and tight sand reservoirs can be found in this association, offering good reservoir prospects. Tidal flats formed during late transgressive events and highstand normal regression due to sufficient sedimentation driven by relatively high tectonic activity (Figs. 4 and 5).

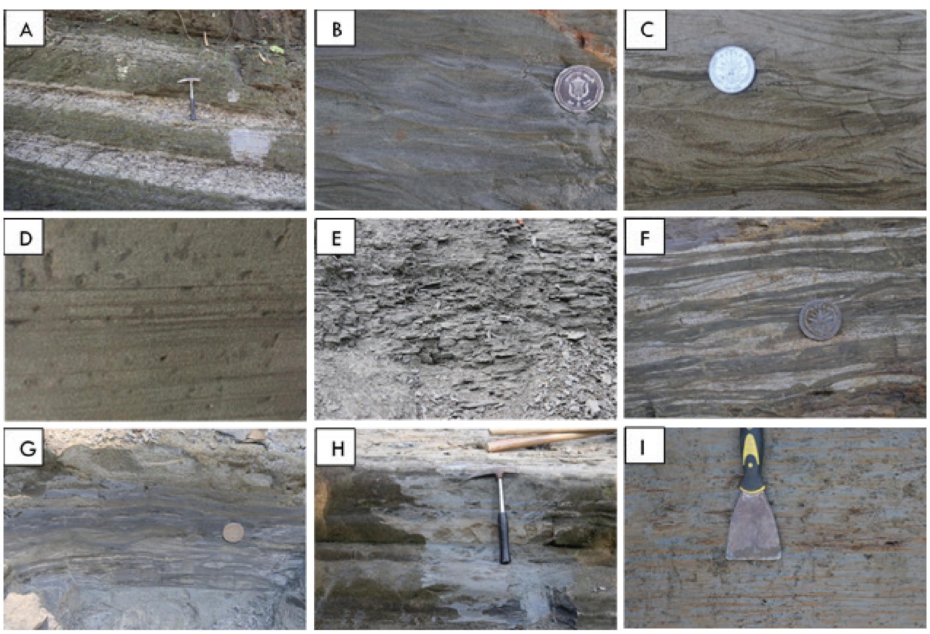

Figure 4: A) Heterolithic Bedding in Navy Road Cut Section (Upper to Middle Surma Group), B) Ripple Cross Bedding in Shilchari Section (Lower to Middle Surma Group) C) Cross Laminated Sandstone in Shilichari Section (Middle Surma Group) D) Parallel Bedded Sandstone in Boroichari Section (Middle to Upper Surma Group) E) Fissile Shale in Shilchari Section (Lower to Middle Surma Group) F) Wavy Bedding in Navy Road Cut Section (Upper to Middle Surma Group) G) Lenticular Bedding in Boroichari Section (Middle Surma Group) H) Tidal Flat Deposits in Navy Road Cut Section (Upper to Middle Surma Group) I) Thinly Laminated Sandstone in Boroichari Section (Middle Surma Group)

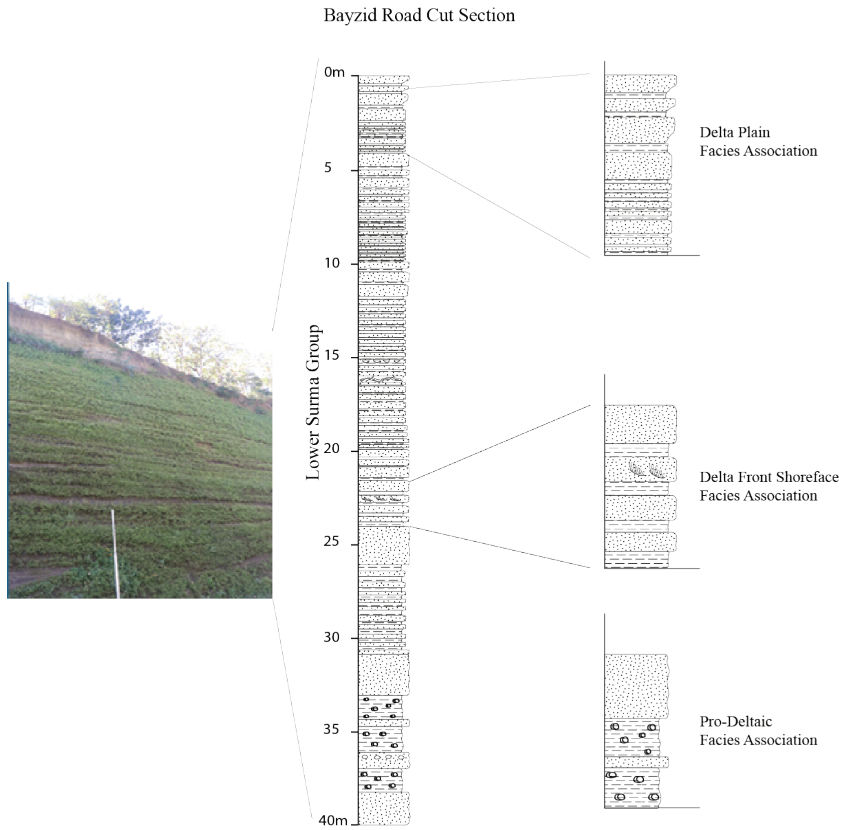

Figure 5: Lithologic Column of the Bayzid Road Cut Section, Sitakund, Representing Facies Associations

Pro-Deltaic Facies Association

A pro-deltaic environment is characterized by the presence of fissile shale, shale with silt streaks, and nodular shale with current ripple siltstone. When the depositional environment is unaltered, the subordinate claystone, heterolithic bedding, and sporadic calcareous bands belong to this shaly unit, which is deposited from suspension. This association is more suitable for unconventional reservoirs. Predominant pro-deltaic sedimentation in shallow marine settings suggests a significant base-level rise, indicating transgressive events. Relatively, a quiet tectonic activity facilitated base-level transgression by generating accommodation space that surpasses the sediment supply (Figs. 6 and 8).

Tidal-Influenced Channel Fill Facies Association

This facies association comprises channel lag deposits, massive to thick-bedded sandstone, trough cross-bedded sandstone, parallel- and ripple-laminated sandstone, and intermittent heterolithic beds. Conventional sandstone reservoirs and channel sands combine to make the reservoir zones in this facies association. Tidal creeks and channels developed during lowstand normal regression and were later back-filled due to tidal activities during transgressive events to form the channel fill facies (Figs. 6 and 7).

Channel Bypass Sand Fill Facies Association

The thin-bed facies association comprises alternating beds of fine to very fine-grained sandstone and mudstone. Sand is transported in shallow marine settings through bypass channels as mud-rich debris flows. Upon reaching the shallow marine setting, the mud settles down to form mudstones, and sand is deposited at the top of the mudstone, as observed in the Labanakhya Chara-Shohosraw Dhara section. The alternating sand beds range from 30 cm to 70 cm, while the shale varies from 5 to 30cm. The well-sorted sand facies are suitable as an unconventional reservoir, with moderate porosity (8-12%) and good permeability. The intermittent tectonic activities within the transgressive event triggered the conduits in the marine depositional system. The depositional trend resembles cyclic sedimentation in the thin-bed facies association through the bypass channels (Figs. 6, 7, and 8).

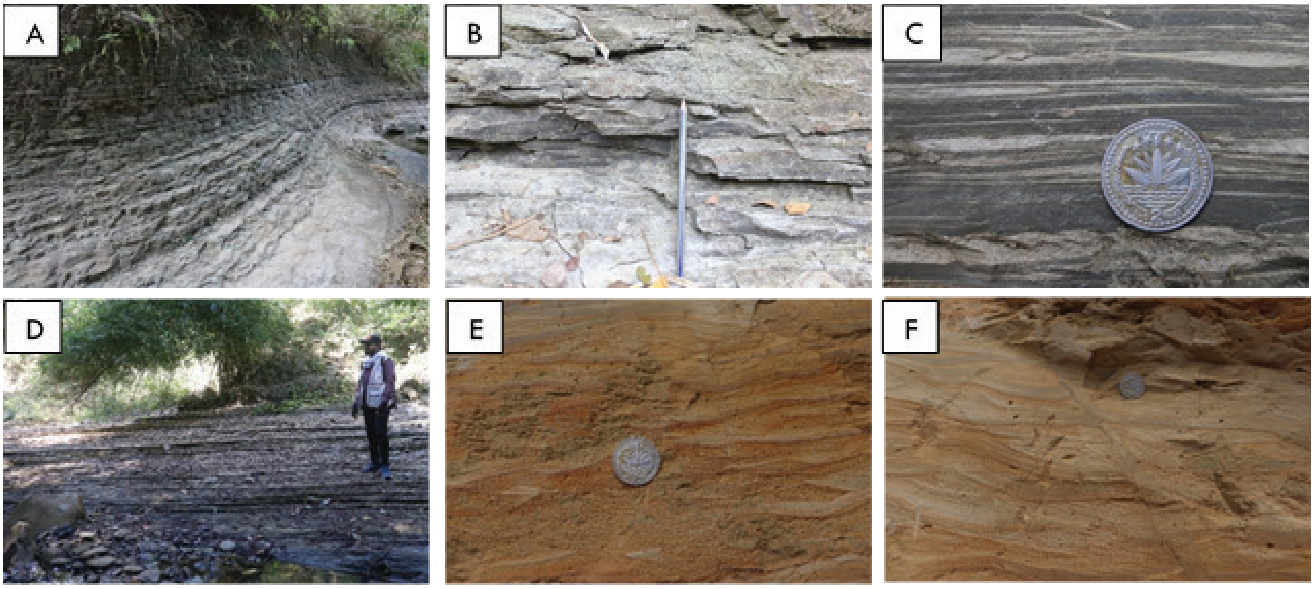

Figure 6: A) Current Ripple Siltstone in Bayezid Road Cut Section (Middle Surma Group), B) Mudstone (Lower Surma Group), C) Shale with Silt Streak in Baraichari Section (Lower Surma Group), D) Planar Thin Beds in Shilchari section, Kaptai (Lower to Middle Surma Group), E) Ripple Laminated Sandstone in Bayezid Road Cut Section (Upper Surma Group), F) Trough Cross Bedded Sandstone in Bayezid Road Cut Section (Upper Surma Group)

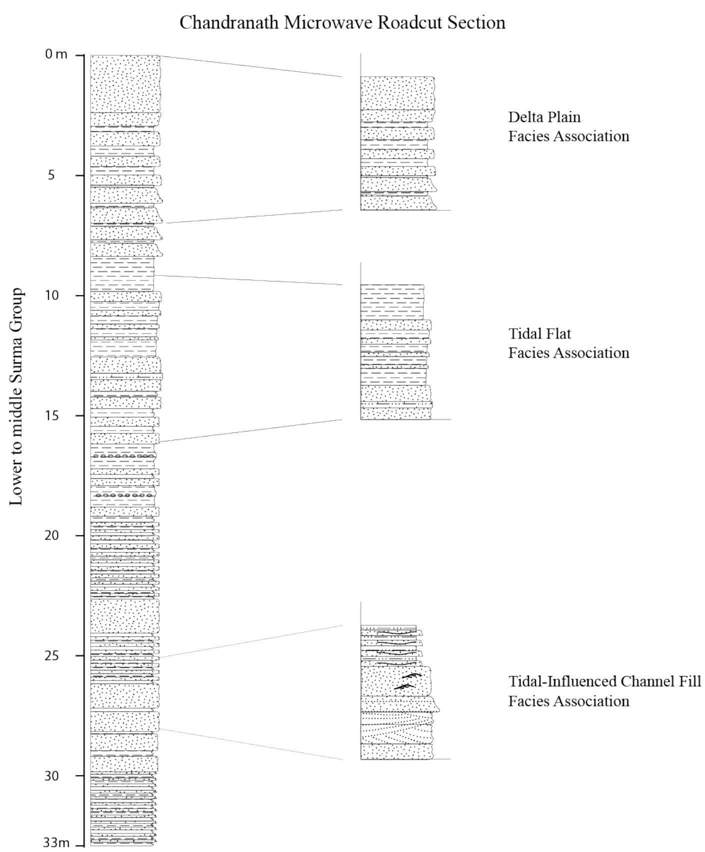

Figure 7: Lithologic Column of the Chandranath Microwave Road Cut Section, Sitakund, Representing Facies Associations

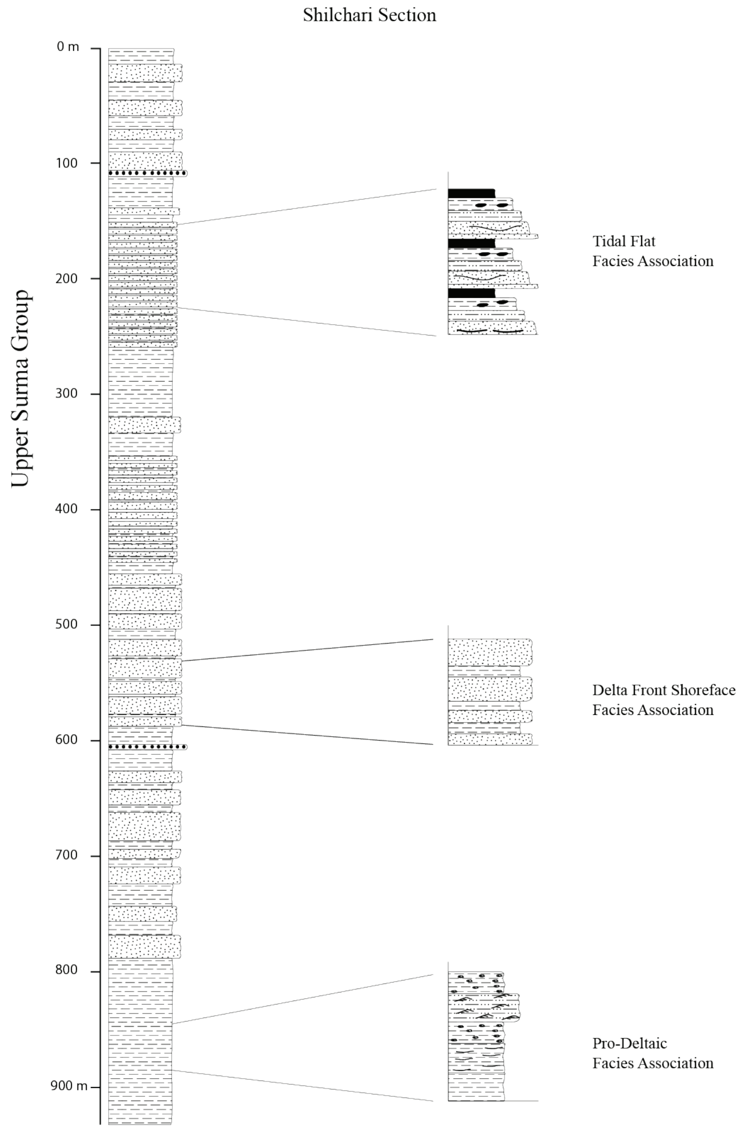

Figure 8: Lithologic Column of the Shilchari Section, Kaptai, Representing Facies Associations

PETROGRAPHIC ANALYSIS

Surma Group sandstones from Sitakund Anticline reveal that 42% of the total samples are medium to fine-grained, 33 % are fine-grained, and 25% are fine to very fine-grained. Also, Surma Group sandstones from Sitapahar Anticline reveal that 15% of the total samples are coarse to medium-grained, 45% are medium to fine-grained, 27% are fine-grained, and 13% are fine to very fine-grained. The roundness and sphericity of the grains were estimated using a visual comparison chart (Powers, 1982). Most of the grains are subangular to subrounded and subspherical to subprismoidal.

The porosity measurement from thin section is always lower than the porosity value determined from the porosimeter, with an average difference of 13.5 % (Stanton, 1977). For the thin sections of the Sitakund structure, the porosity ranges from 7% to 21%. On the other hand, the porosity for the thin sections of the Sitapahar structure ranges from 5% to 23%. (Table 3)

Table 3: Textural Properties of the Surma Group Sandstone Samples from the Sitakund Structure (ST) and Sitapahar Structure (SP) Obtained from Thin-Section Microscopic Study

Sample No.	Grain Size	Grain Shape	Grain Sorting	% Thin section porosity	% Matrix
ST-1	Med.-Fine	Sub rounded to sub angular	Moderate	13	1
ST-2	Med.-Fine	Sub rounded to sub angular	Moderate	15	2
ST-3	Med.-Fine	Sub rounded to sub angular	Moderate-Well	21	2
ST-4	Med.-Fine	Sub rounded to sub angular	Moderate	18	1
ST-5	Fine	Sub rounded to sub angular	Moderate-Well	8	2
ST-6	Fine	Sub rounded to sub angular	Moderate-Well	9	1
ST-7	Fine-V. Fine	Sub rounded to sub angular	Moderate-Well	7	2
SP-1	Med.-Fine	Angular to sub-rounded	Moderate	18	3
SP-2	Med.-Fine	Sub angular to sub-rounded	Moderate- Poor	12	2
SP-3	Med.	Sub angular to sub rounded	Moderate- Well	5	2
SP-4	Med.-Fine	Sub angular to sub rounded	Moderate- Well	20	3
SP-5	Med.-Coarse	Angular to sub angular	Well	23	1
SP-6	Med.-Fine	Sub rounded to sub angular	Well	8	2
SP-7	Med.-Fine	Sub rounded to sub angular	V. Well-Well	10	3

Quartz-Mica Tectonite comprises 13% to 25% of the total lithic grains. Quartz-Mica-Graphite Tectonite makes up 2% to 15% of total lithic grains. Mica Tectonite is a minor component, comprising 2% to 10% of the total lithic grains. Foliated Metaquartzites make up 1% to 10% of total lithic grains. Volcanic lithic grains are produced from the fragmentation of volcanic rocks and contain crystals of quartz, feldspar, ferromagnesian minerals, and opaque minerals. A cluster of feldspar laths can be seen, and they are aligned in the direction of these grains. Felsitic, microlithic, and lathwork textures are common in volcanic lithic grains but are rarely observed. Indeterminate lithic grains don't fall within the above categories and exhibit a strange and unknown nature. They constitute 4% to 8% of the total lithic grains (Fig. 9).

Point count data shows that feldspar constitutes 0% to 4% of the total rock components. The studied sandstone samples contain both plagioclase and potassium feldspars, which are more common, but orthoclase and microcline are also present (Fig. 10).

Studied sandstone samples contain chlorite, one of the most common detrital materials. It can occur as large detrital flakes (0.2-0.5 mm) that spread out at the ends and show a characteristic green color with strong pleochroism (Fig. 11). Muscovite is more abundant than biotite in the studied samples. Chlorite and Mica comprise 4% to 10% of total rock components (Fig. 11). Chlorite is most common in the sandstone samples. They can occur in three different modes: i) as grain coating on the detrital grains, which is known as chlorite rims; ii) as pore-filling materials; and iii) as replacing materials (Fig. 12).

Due to its very fine nature, it is difficult to determine the matrix mineralogy. However, quartz and clay minerals are identified, and the total matrix content is lower than 5% in the studied thin sections. Altered detrital micas, crushed shale, mudstone, and deformation of soft lithic grains can remain as discontinuous interstitial paste and form a pseudomatrix. Point counting data show that sandstones from the Sitakund anticline contain only 0.1% to 2% kaolinite, but sandstones from Kaptai rarely show kaolinite in petrographic studies. Illites are minor diagenetic clay minerals and are related to pressure solutions.

Authigenic quartz forms due to diagenesis in the lower units of the Surma Group deposits, acting as quartz overgrowth cements. Quartz overgrowth cements make up 1% to 3% of the samples from the Sitakund anticline and 3% to 5% of the samples from the Sitapahar anticline. Surma Group sandstone samples from the Sitakund and Sitapahar anticlines contain a lot of calcite cement. Calcite cement makes up 0% to 35% of Sitakund and Sitapahar anticline samples (Fig. 13).

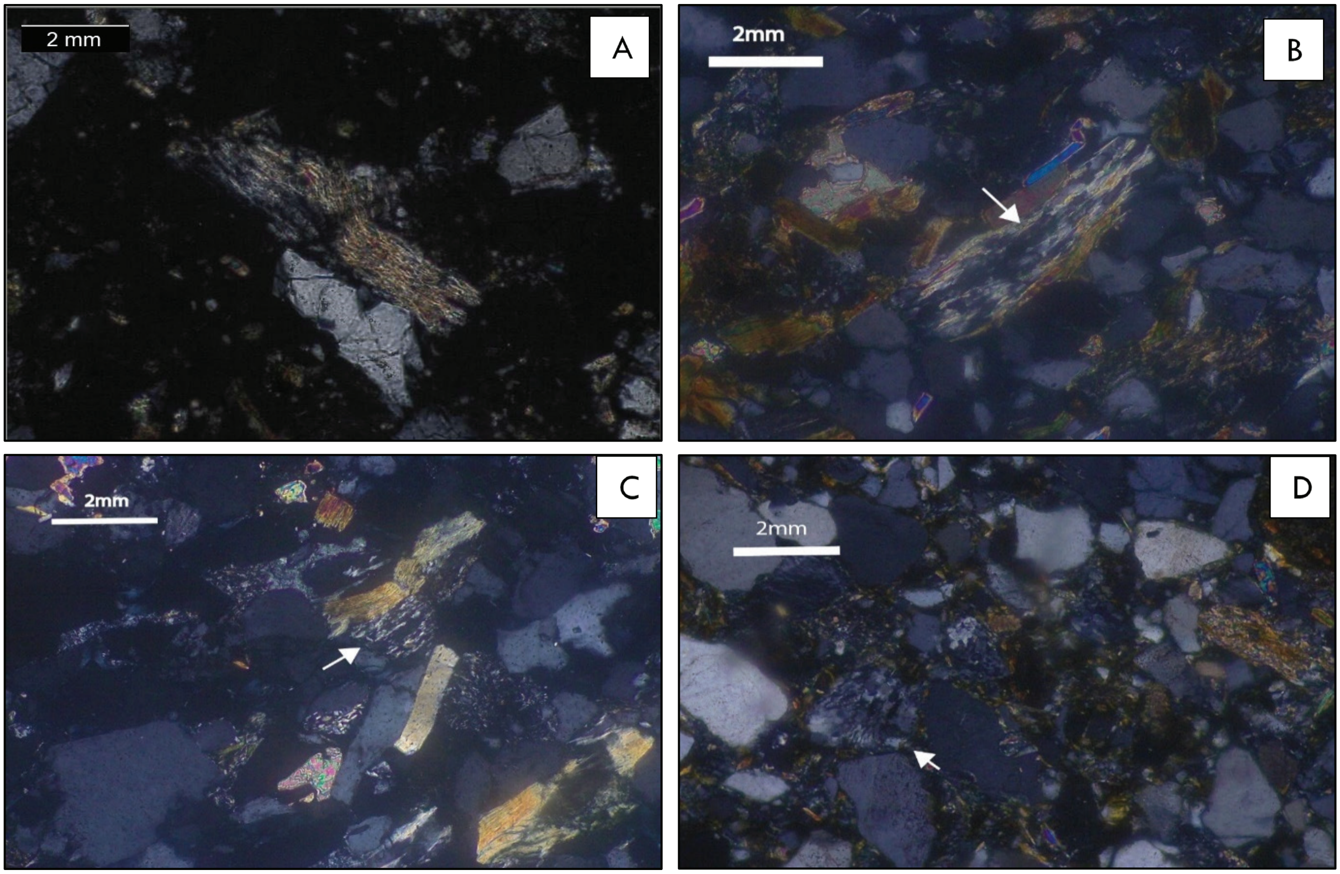

Figure 9: Photomicrograph of A) Quartz-mica Tectonite from Upper Surma Group in Kaptai, B) Quartz-mica-graphite Tectonite from Upper Surma Group in Kaptai, C) Mica Tectonite from Upper Surma Group in Sitakund, D) Metaquartzite arrowed from Upper Surma Group in Kaptai. Crossed Nicols

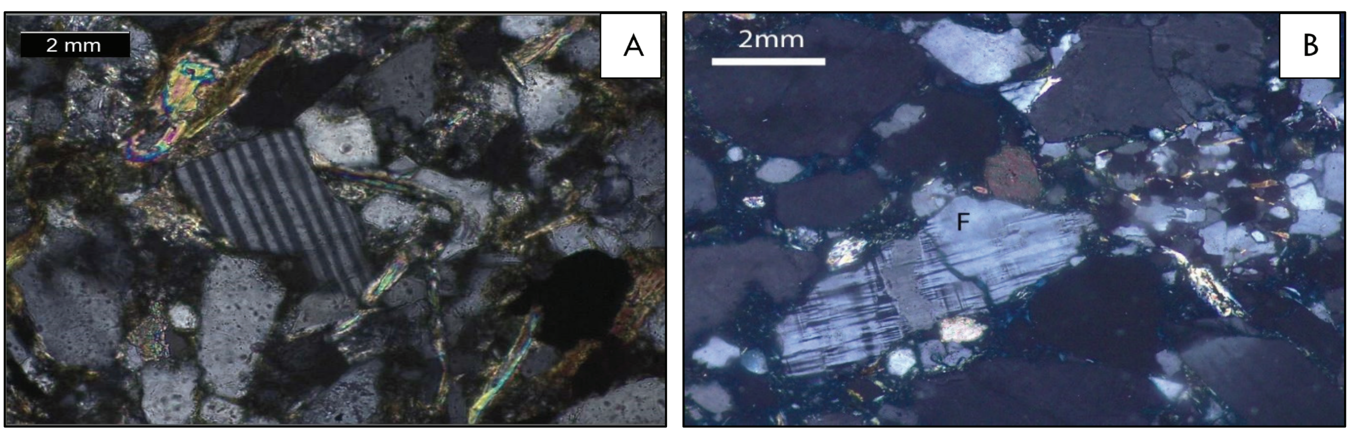

Figure 10: Photomicrograph of A) Plagioclase Feldspar with Polysynthetic Twinning from Upper Surma Group in Sitakund, B) Microcline with Cross-Hatch Twinning from Upper Surma Group in Sitakund. Crossed Nicols

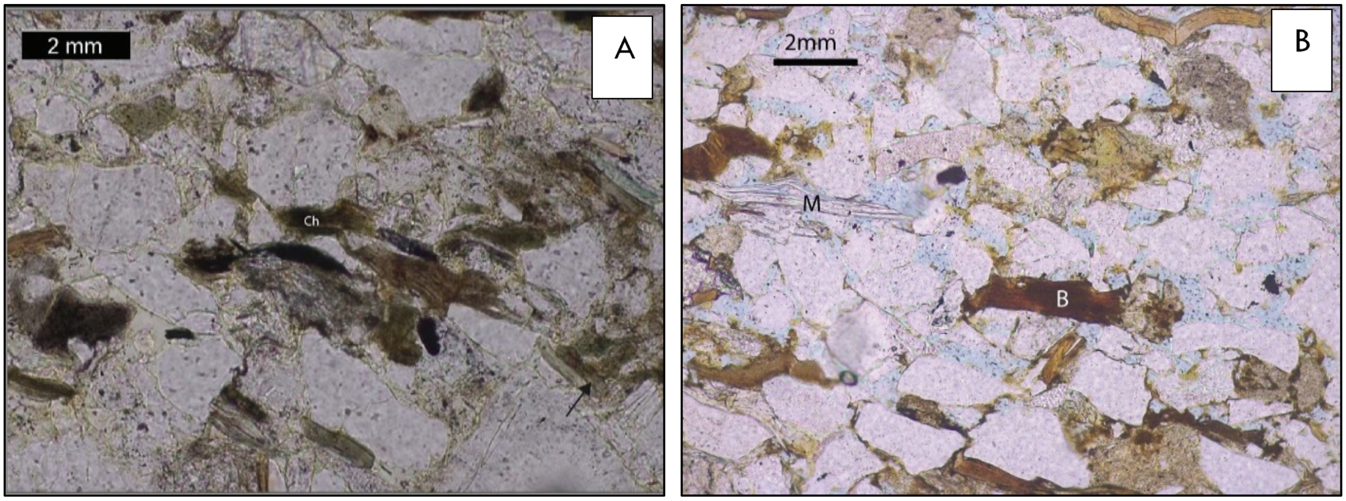

Figure 11: Photomicrograph of A) Detrital Chlorite (Ch) and Pore-Filling Chlorite Cement (arrowed) from Lower Surma Group in Sitakund, B) Detrital Biotite (B) (deep brown) and Mica (M) from Upper Surma Group in Sitakund Under Plane-Polarized Light

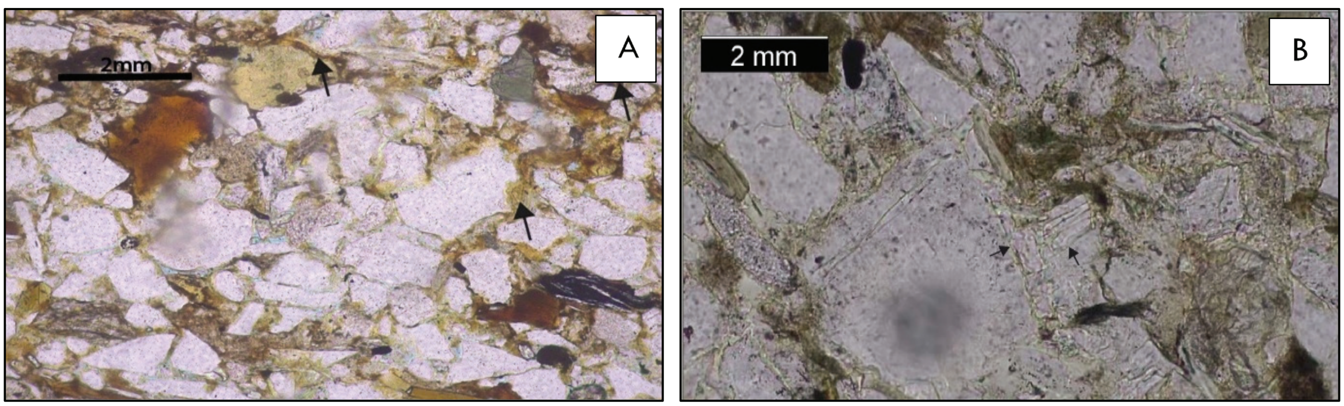

Figure 12: Photomicrograph of A) Pore-Filling Chlorite (green) and Grain-Coating Chlorite (green), B) Detrital Biotite (B) Replacement of Feldspar Along Cleavage by Chlorite from Upper Surma Group in Sitakund Under Plane-Polarized Light

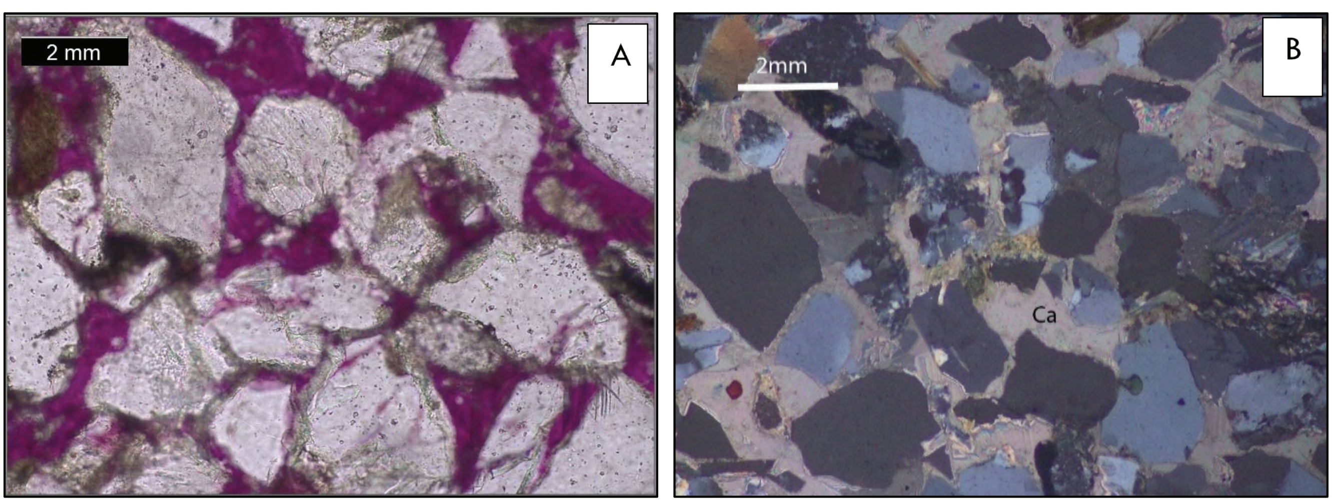

Figure 13: Photomicrograph Showing A) Isolated Pore-Filling Calcite Cement (stained) from Lower Surma Group. Plane Light, (B) Poikilotopic Calcite Cement (Ca) from Upper Surma Group in Sitakund Under Crossed Nicols

Classification and Nomenclature of the Surma Group Sandstones

Samples from both locations are classified as clean sands (arenites) due to their matrix quantity being less than 15%. Quartz, feldspars, and lithic grains are recalculated to 100% (Table 4) and plotted on the triangular diagrams (Fig. 14 & 15) where Neogene Surma Group sandstones are sublitharenites.

Table 4: Relative Abundance of Quartz, Feldspar, and Lithic Grains (Recalculated to 100%) for Surma Group Sandstones

Sample No.	Quartz	Feldspar	Lithic
ST-1	79	7	14
ST-2	81	3	16
ST-3	77	4	19
ST-4	75	4	21
ST-5	80	3	17
ST-6	84	2	14
ST-7	76	2	22
SP-1	83	3	14
SP-2	84	5	11
SP-3	85	3	12
SP-4	81	2	18
SP-5	82	2	16
SP-6	77	5	18
SP-7	78	2	20

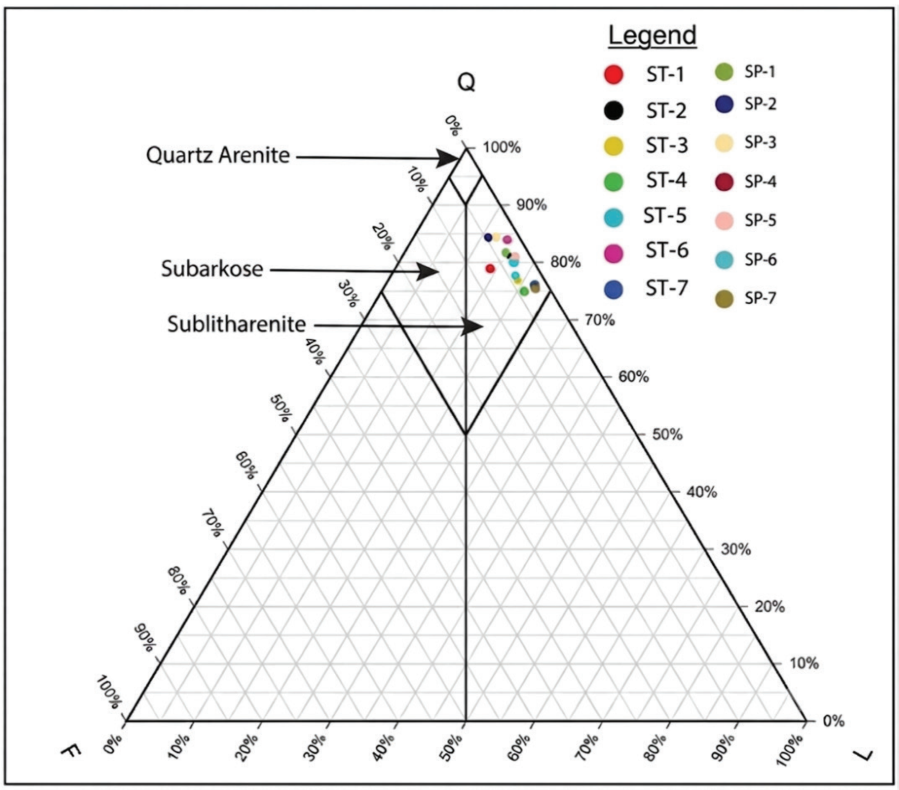

Figure 14: QFL Triangular Plot for Classification of the Studied Sandstone Samples (Dott, 1964). All 14 Sandstone Samples from the Sitakund and Sitapahar Structures Fall Under the Sublitharenite Category

Diagenesis

Surma Group sandstones exhibit a gradual decrease in point contacts and long contacts with increasing depth, where concavo-convex and sutured contacts are abundant, as other processes, rather than packing readjustment, play a significant role (Fig. 15). This sandstone contains various ductile grains, such as shale, claystone, siltstone, and schist fragments, and is permanently deformed due to overburden pressure. These grains are squeezed between adjacent rigid grains, and flow into adjacent pore spaces is very common due to overburden pressure. The grains lose shape in this process and form an interstitial matrix known as a pseudomatrix (Fig. 16A).

The sandstone also contains ample examples of flexing flexible minerals, such as mica and chlorite, and fracturing brittle grains, including feldspars (Fig. 16 B and C), lithic grains, or heavy minerals. Based on the gradual increase of overburden pressure, mica flakes can be gently curved, with some fracturing in extreme cases. Feldspars are generally fractured along cleavage planes, but brittle lithic grains show more fracturing (Fig. 16D).

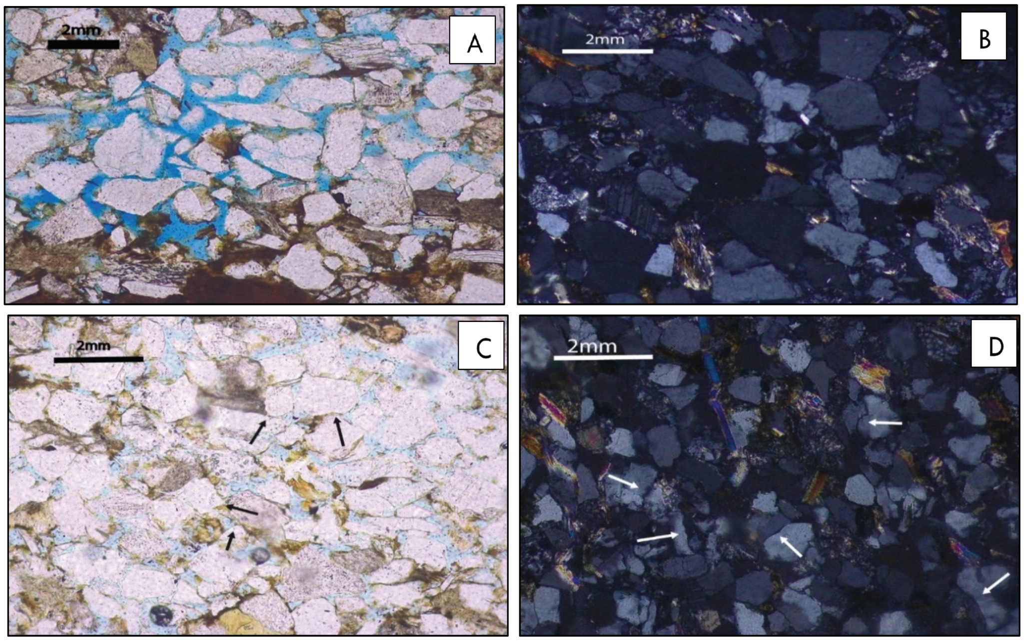

Figure 15: Photomicrograph Showing A) Very Loose Packing of Grains from the Upper Surma Group in Kaptai. Plane Light.B) Very Tight Packing of Grains from the Upper Surma Group in Kaptai. Crossed Nicols, C) Point Contacts (arrowed) between Detrital Grains from the Upper Surma Group in Kaptai. Plane Light, D) Straight, Sutured, and Concavo-Convex Contacts (arrowed) between Detrital Grains from Upper Surma Group in Kaptai. Crossed Nicols

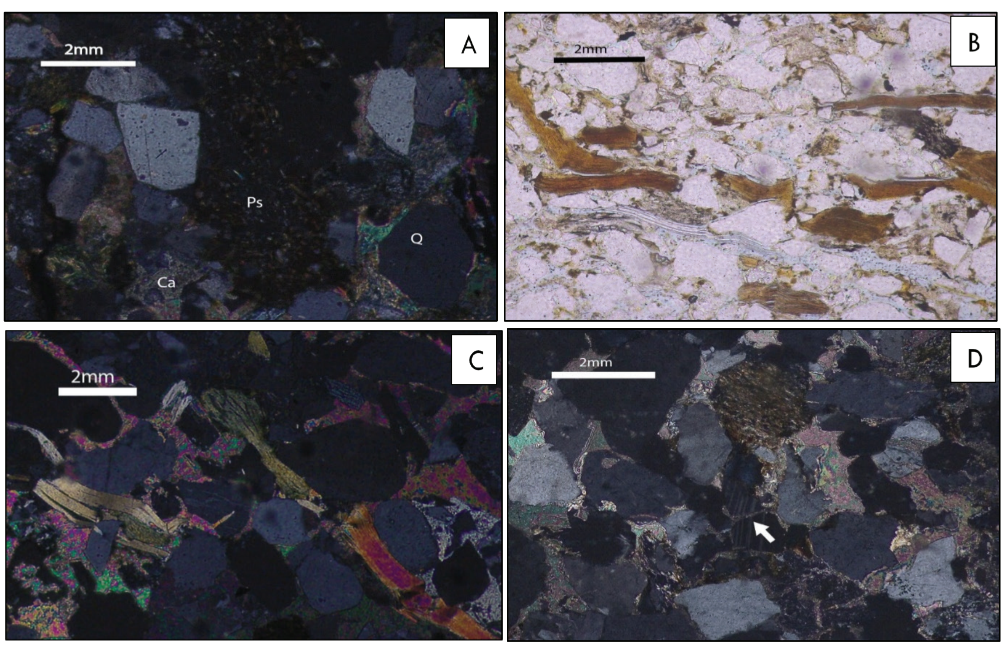

Figure 16: Photomicrograph Showing A) Pseudomatrix in Kaptai. Crossed Nicols, B) Fractured Chlorite due to Bending in Kaptai. Plane Light. C) Bended and Partly Fractured Mica from in Kaptai. Crosses Nicols. D) Fractured Feldspar in Kaptai. Crossed Nicols

The presence of pressure solution is observed in the studied samples, which increases the compaction of rocks and tight packing of grains due to increasing stress at their grain contacts (Fig. 17A). Quartz overgrowth is one of the prominent forms of cementation observed in the lower parts of the studied samples (Fig. 17B). The studied samples predominantly contain ferroan calcite cements. Grain-coating chlorites (chlorite rims) and pore-filling chlorites are predominant in the studied samples, but replacements of chlorite cement are rarely found in some samples. The textural relationship of chlorite cement and other authigenic minerals suggests that chlorite cement is of the early generation of diagenetic phases. Surma Group deposits show kaolinite cement at the lower parts of the rock sequence, as kaolinite cementation is the last diagenetic phase (Fig. 17C, D).

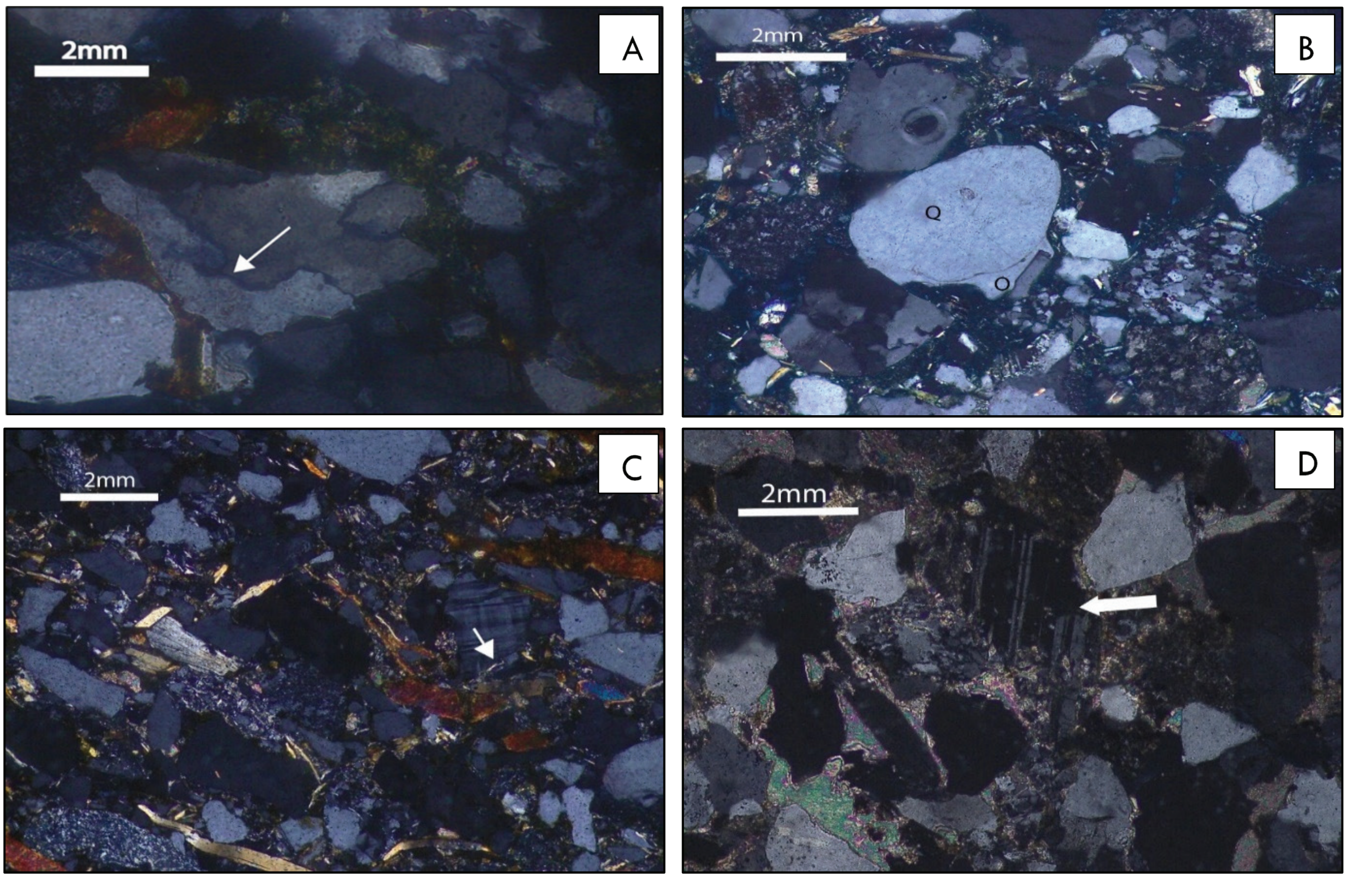

Figure 17: Photomicrograph of A) Sutured Contact, Developed due to Pressure Solution Under Crossed Nicols, B) Advanced Terminated Type of Quartz Overgrowth, Crossed Nicols. C) and D) In Situ Alteration of Feldspar into Kaolinite Under Crossed Nicols

The studied Surma Group sediments contain evidence of replacement predominantly by calcite and, in some cases, by chlorite. According to the studied samples, quartz, feldspars (silicate minerals), and other lithic grains undergo replacement (Fig. 18A). Alteration is also present in the studied samples. Biotite is altered by chlorite and is commonly referred to as chloritized biotite (Fig. 18B). Greenish tints along cracks or cleavage accompany its flaky nature and brownish color.

The studied samples exhibit dissolution features in the deeper part. The studied samples show feldspar dissolution in a greater amount than other grains. Calcite dissolution is only observed in the late diagenetic isolated pore-filling cement of the studied samples. Early poikilotopic ferroan calcite cement does not exhibit any dissolution, as it fills the pore spaces and prevents pore fluid percolation (Fig. 19).

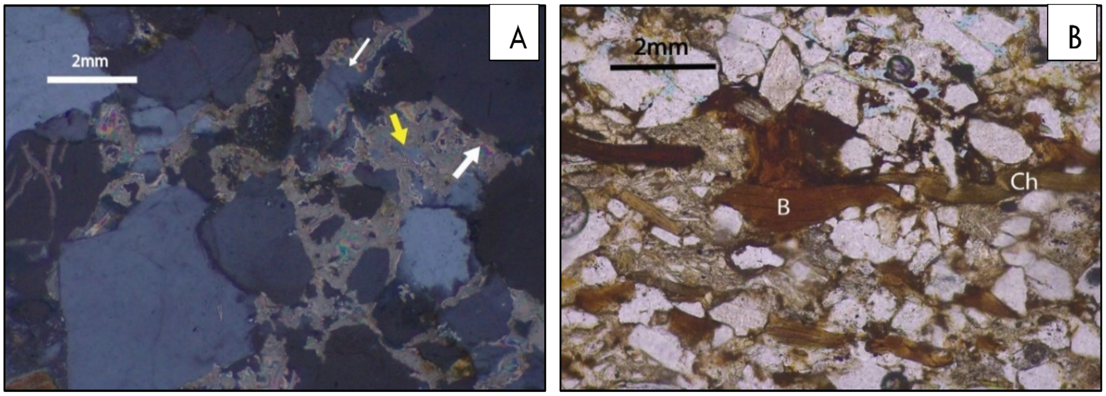

Figure 18: Photomicrograph of A) Corroded (quartz) Grain Replaced by Calcite Indicated by White Arrow and Remnant Replacement Shown by Yellow Arrow. Crossed Nicols, B) Chloritized Biotite (b), Chlorite (Ch), Under Crossed Nicols

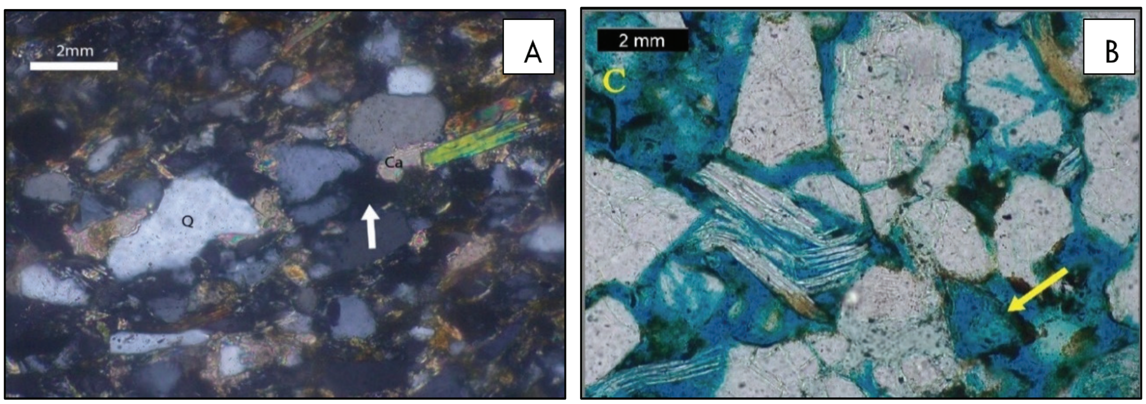

Figure 19: Photomicrograph Showing A) The Partial Dissolution of Calcite Cement (arrowed) and Isolated Pore-Filling Fe-Calcite. Q. Quartz, Ca. Crossed Nicols, B) Evidence of Extensive Dissolution of Feldspar, Mouldic Secondary Porosity with a Clay-Mineral Rim (arrowed), and Partial Dissolution of Mica. Plane Light

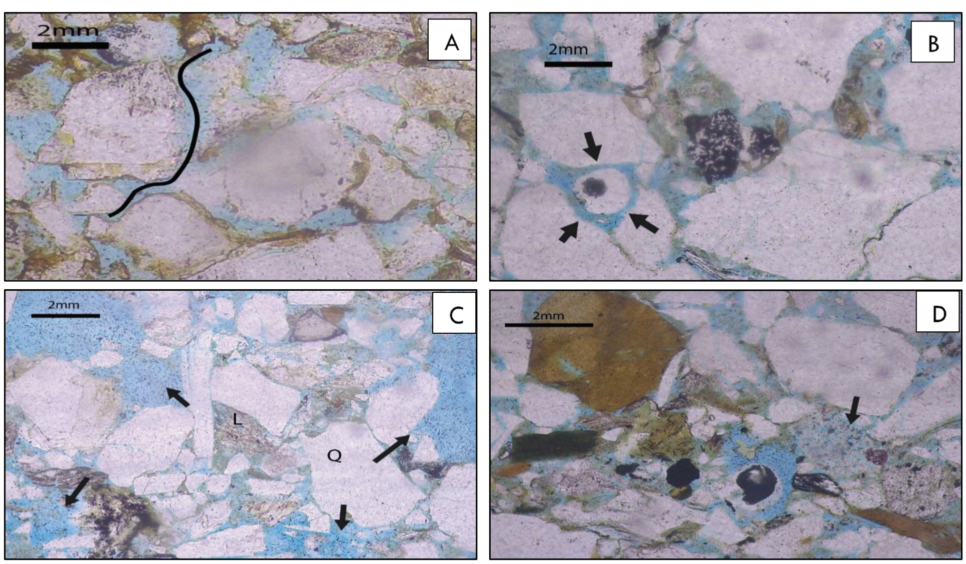

Figure 20: Photomicrograph Showing A) Elongated Pore Space, Plane Light. B) Floating Grain (arrowed) Plane Light. C) Oversized Pore Space (arrowed) and Floating Grain. Plane Light. D) Skeletal Replacement of Lithic Grain (arrowed). Plane Light

Dissolution significantly enhances secondary porosity in the Surma Group sandstones by removing feldspars, lithic fragments, replacive calcite, and authigenic cements such as calcite and dolomite. Partial to complete dissolution of feldspar and lithic grains by acidic pore fluids generates oversized, elongated, and intracement pores (Fig. 20), with some samples showing dissolution of more than 50% of feldspar grains. Skeletal grains commonly exhibit partial dissolution, whereas complete dissolution produces oversized secondary pores. Minor quartz dissolution is also locally observed. Dissolution of late ferroan and replacive calcite is evidenced by floating and corroded grains, heterogeneous grain packing, remnant cement stains, and partially dissolved cement phases (Fig. 20).

The determined paragenetic sequence is shown in Fig. 21.

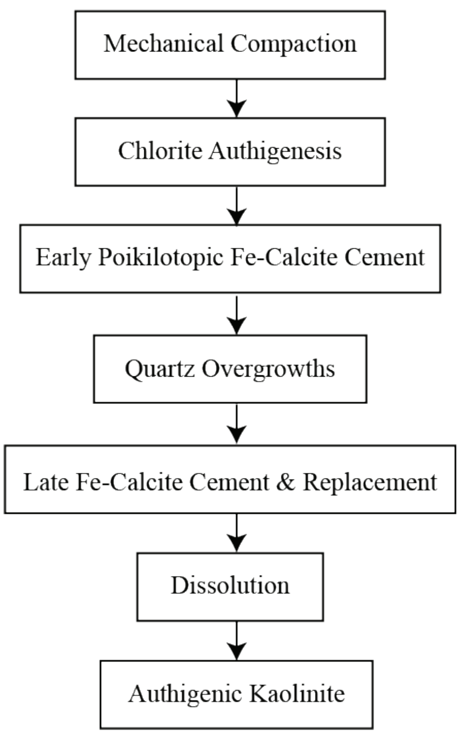

Figure 21: Paragenetic Sequence of the Collected Sandstone Samples of Sitakund

FE-SEM and EDS ANALYSES

The samples ST-1, ST-3, SP-2, and SP-4 contain a combination of visible minerals, including quartz, feldspar, kaolinite, mica, and smectite. Four SEM images for sample ST-1 have been analyzed, where micropores show good intragranular pore space due to dissolution, connected intergranular pore spaces are more frequently noticed, detrital quartz along with quartz overgrowth showing illite dust line, detrital feldspar along with kaolinite from dissolution and decomposition of feldspar, and grain coating chlorite (Fig. 22A).

Calcite cementation due to dissolution and precipitation, quartz overgrowth, pore-lining illite-smectite mixed layer, and pore-filling chlorite are present (Fig.22B). Therefore, pore throat diameter reduction due to coating disrupts intergranular pore connections. Still, overall, a good interconnection between intergranular pore spaces is observed. Chloritized biotite is evident from thin-section petrography. Abundant Intragranular pore spaces, some intragranular micropores due to dissolution, calcite cementation, illite-smectite mixed layers bridging pore throats, and chlorite coating are also present (Fig. 22C). Grain size is medium to coarse in the SEM images. Mica bending due to compaction, pore filling, calcite cementation, foraminifera microorganisms, and little matrix are observed (Fig. 22D). There is a reasonable degree of porosity, and intergranular pore spaces are available. Still, cementing material decreases the porosity in some parts.

The chemical compositions of the selected spots show that the minerals of the studied spots are composed of Carbon(C), Oxygen (O), Sodium (Na), Magnesium (Mg), Aluminum (Al), Silicon (Si), Potassium (K), Calcium (Ca), and Iron (Fe) (Fig. 23). The SEM images for sample ST-3 have been analyzed, revealing an abundance of pore space, intergranular pore connections, pore lining, pore filling, and grain coating with chlorite, detrital quartz, minor quartz overgrowth, and calcite cement (Fig. 24).

EDS Spot analysis shows that the O and Si mass percentages are 65.48% and 28.05%, respectively. Their atomic percentages are 74.02 and 18.06, respectively. Here, oxygen and silicon are more abundant than the other components, but overall, the components suggest it is a Silicate group mineral. Spot 003 shows the presence of O, C, Si, K, Fe, and Al, with mass percentages of 54.51%, 3.24%, 30.22%, 2.84%, 1.82%, and 5.66%, respectively. Their atomic percentages are 66.27%, 5.25%, 20.93%, 1.41%, 0.63%, and 4.08%, respectively. Overall, the components suggest it is a mineral of the Clay Group of the Phyllosilicates subclass (Fig. 25).

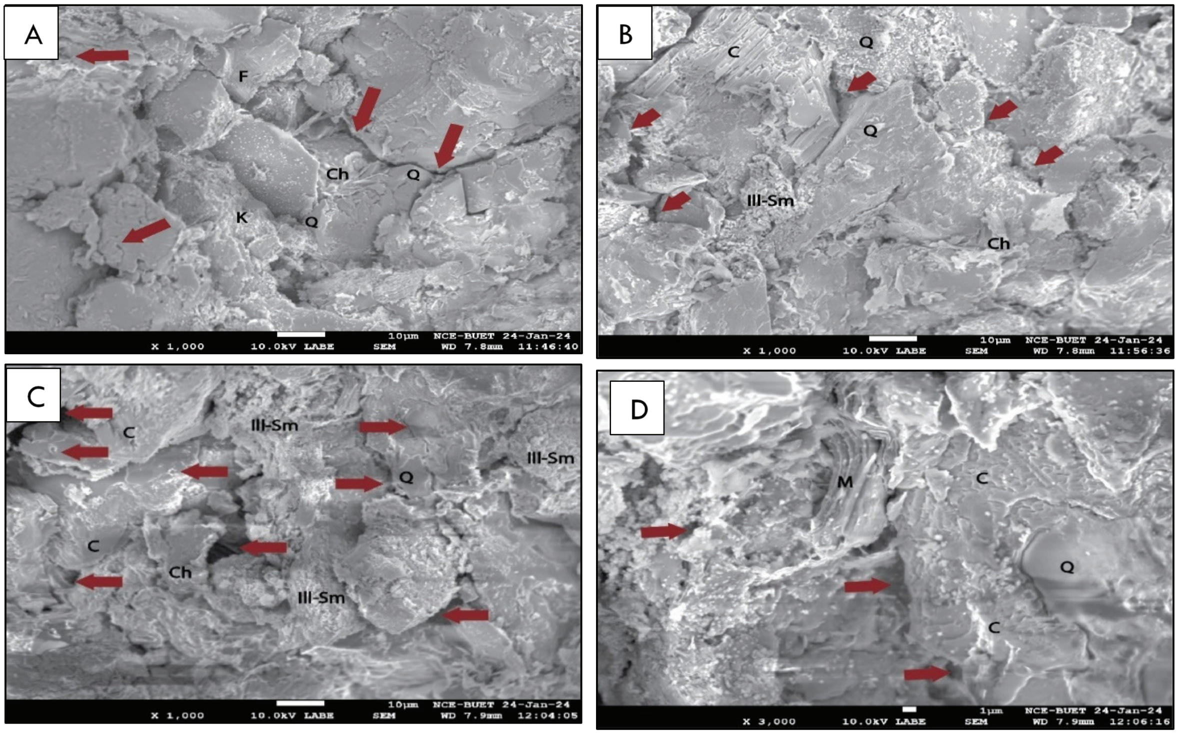

Figure 22: Scanning Electron Micrographs of Surma Group Sandstones Showing Kaolinite, Feldspar, Quartz, Along with Quartz Overgrowth Separated by Illite Dustline, Grain-Coating Chlorite Platelets (A); Calcite Cementation, Quartz, Pore Filling Chlorite, and Illite-Smectite Mixed Layer (B & C); Mica Bending, Pore Filling Calcite Cement, and Quartz (D). Brown Arrows Indicate Intragranular Micropores Resulting from Dissolution, which are Connected to Intergranular Pore Spaces. The Minerals are Indicated as Q=quartz, C=calcite, Ch=chlorite, F=feldspar, K=kaolinite, M=mica and Ill-Sm= illite-smectite

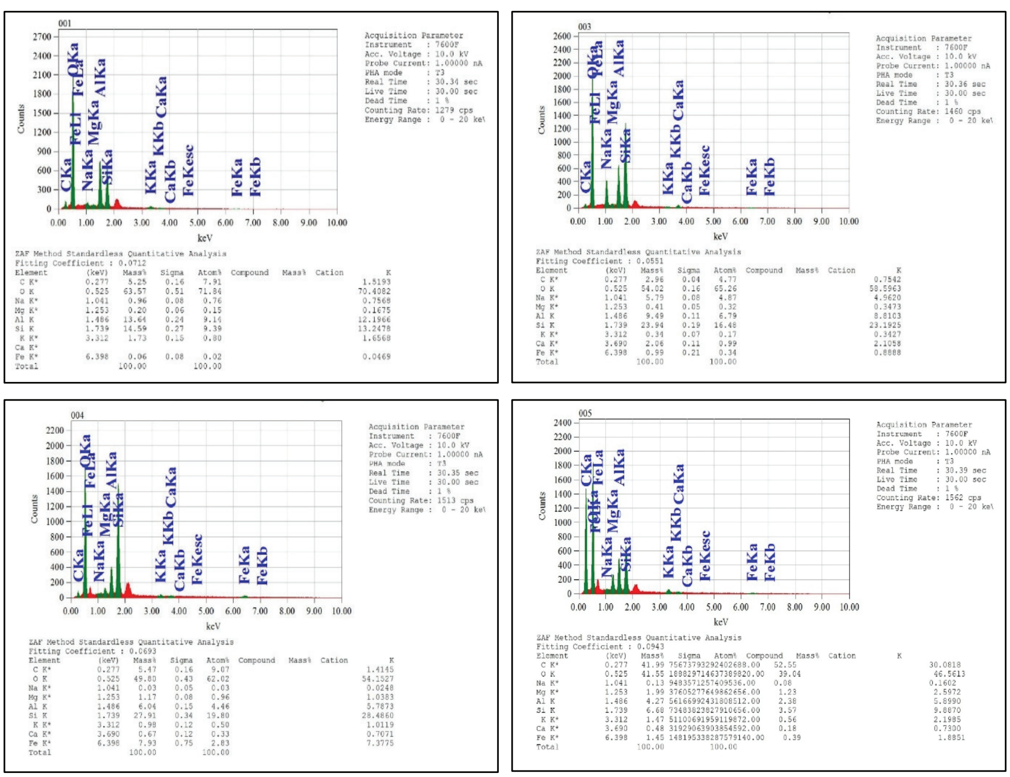

Figure 23: Atomic and Mass Percentage of the Analyzed Chemical Elements of EDS Spot Locations from Sample ST-1

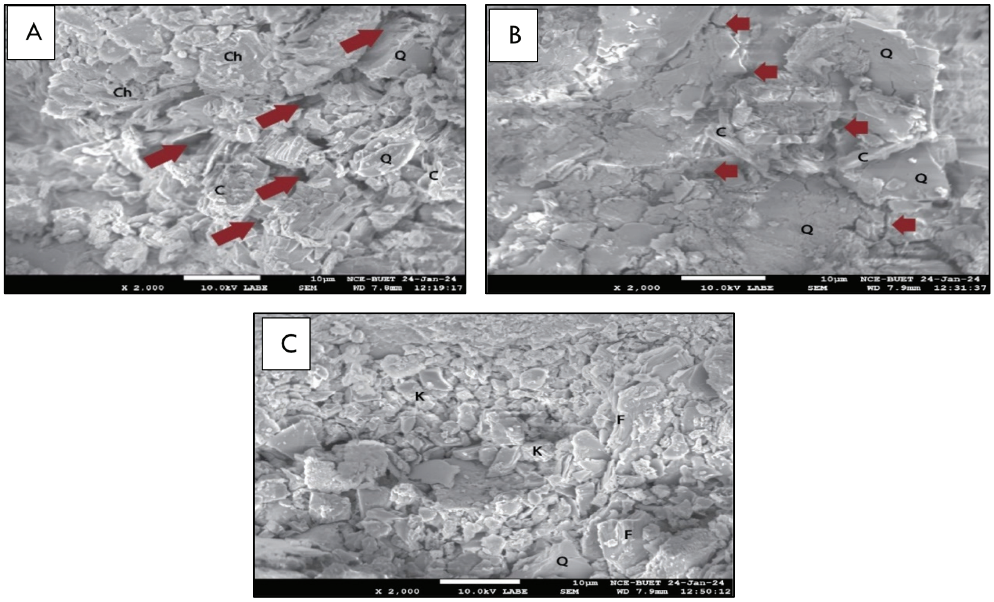

Figure 24: Scanning Electron Micrographs of Surma Group Sandstones Showing Calcite Cementation, Quartz Along with Quartz Overgrowth, Grain-Coating, Pore Bridging or Pore Filling Rosette Type Chlorite (A); Calcite Cementation, and Quartz Grains Containing Microfractures (B); Thin Booklets of Kaolinite Along with Feldspars (C). Brown Arrows Show Connected Intergranular Pore Spaces. The Minerals are Q=Quartz, C=Calcite, Ch=Chlorite, F=Feldspar, and K=Kaolinite

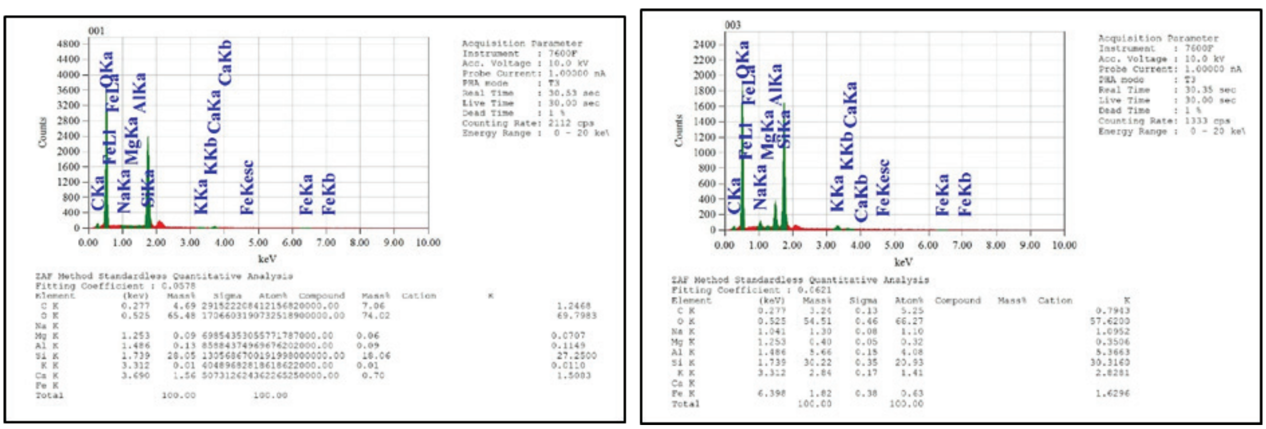

Figure 25: Atomic and Mass Percentage of the Analyzed Chemical Elements of EDS Spot Locations from Sample ST-3

The SEM images have been analyzed for sample SP-2, where hexagonal di-pyramidal quartz overgrowths reduce pore volume and evidence of quartz cementation. A pore-filling illite-smectite mixed layer is present (Fig. 26). A significant reduction in porosity is evident in this figure.

EDS Spot analysis reveals that the mass percentages of O, C, Si, Al, Ca, and Fe are 46.80, 4.06, 4.61, 2.21, 38.62, and 2.31, respectively. Their atomic percentage are 64.08, 7.40, 3.59, 1.80, 21.11, and 0.91, respectively. The components suggest that the mineral belongs to the Plagioclase series of Tectosilicates (Fig. 27). Spot 010 indicates that the mass percentages of O, C, Si, Al, and Ca are 43.58, 15.06, 26.12, 2.02, and 11.84, respectively. Their atomic percentages are 51.24%, 23.59%, 17.49%, 1.41%, and 5.55%, respectively. These components suggest that the mineral belongs to the Plagioclase series Tektosilicates subclass (Fig. 27).

The SEM images have been analyzed for sample SP-4, where detrital quartz, grain coating, rosette chlorite, calcite cementation, and oversized intergranular porosity due to dissolution are present (Fig. 28). Microfracture development in quartz in minor quantities, quartz overgrowth, and an illite-smectite mixed layer (Fig. 28) suggest porosity reduction. However, the overall intergranular pore connection was good in the studied sample.

Spot 002 shows that the mass percentages of O, C, Si, Al, Mg, K, Fe, and Ca are 42.46%, 2.62%, 33.32%, 5.69%, 1.35%, 1.59%, 11.68%, and 1.12%, respectively. Their atomic percentages are 57.58%, 4.72%, 25.75%, 4.57%, 1.20%, 0.88%, 4.54%, and 0.61%, respectively. The components suggest that the mineral belongs to the Clay minerals group, specifically the Phyllosilicates subclass (Fig. 29). Spot 004 indicates that the mass percentages of O, C, Si, Al, and Fe are 16.22, 5.09, 11.20, 3.22, and 62.57, respectively. Their atomic percentages are 32.34%, 13.53%, 12.72%, 3.81%, and 35.73%, respectively. The components suggest that the mineral belongs to the Clay minerals group, specifically the Phyllosilicates subclass (Fig. 29).

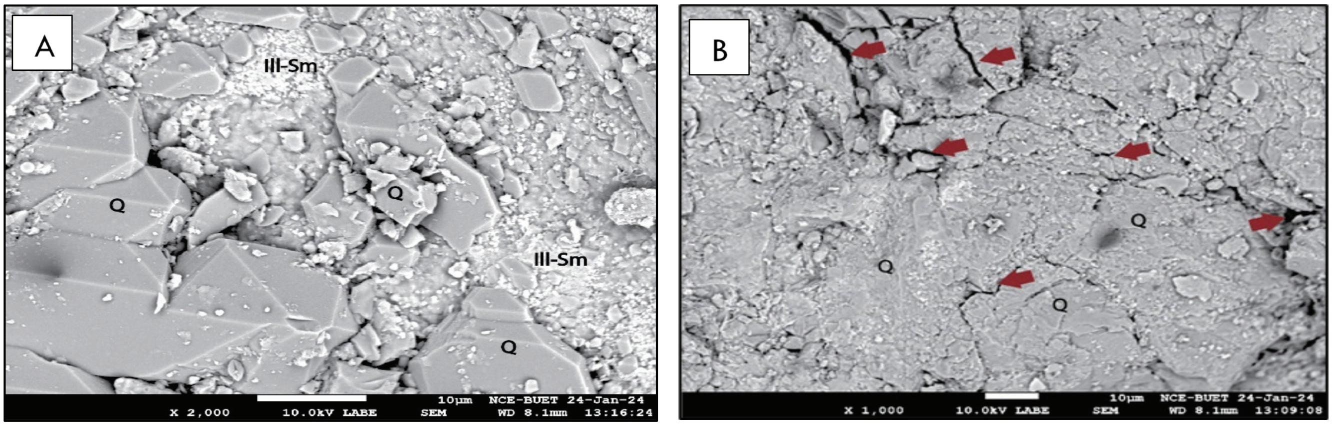

Figure 26: Scanning Electron Micrographs of Surma Group Sandstones Showing Quartz Along with Quartz Overgrowth, Grain-Coating, Pore Bridging, or Pore Filling Illite-Smectite Mixed Layer (A); Quartz Grains Containing Microfractures, Clay Coating in the Grain Surfaces (B). Brown Arrows Show Connected Intergranular Pore Spaces. The Minerals are Indicated as Q=Quartz and Ill-Sm= Illite-Smectite

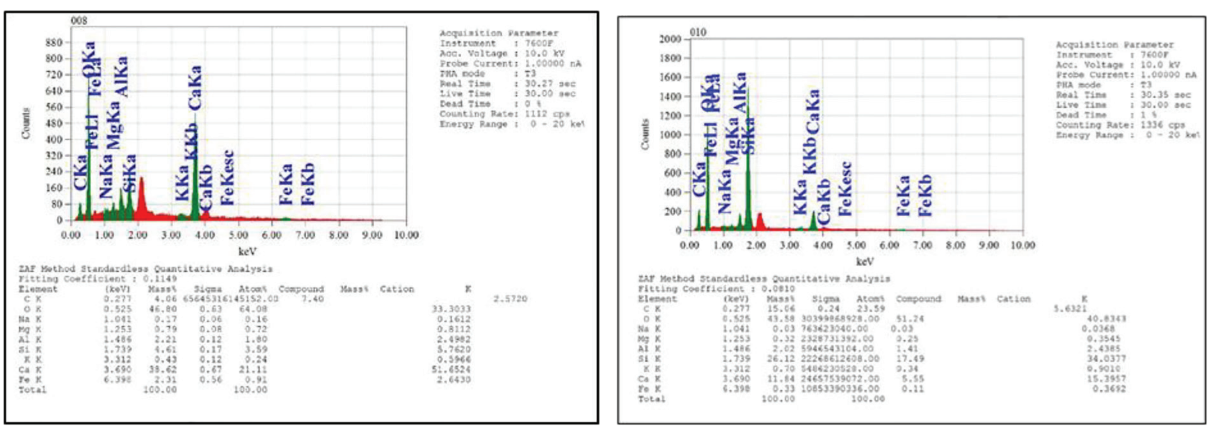

Figure 27: Atomic and Mass Percentage of the Analyzed Chemical Elements of EDS Spot Locations from Sample SP-2

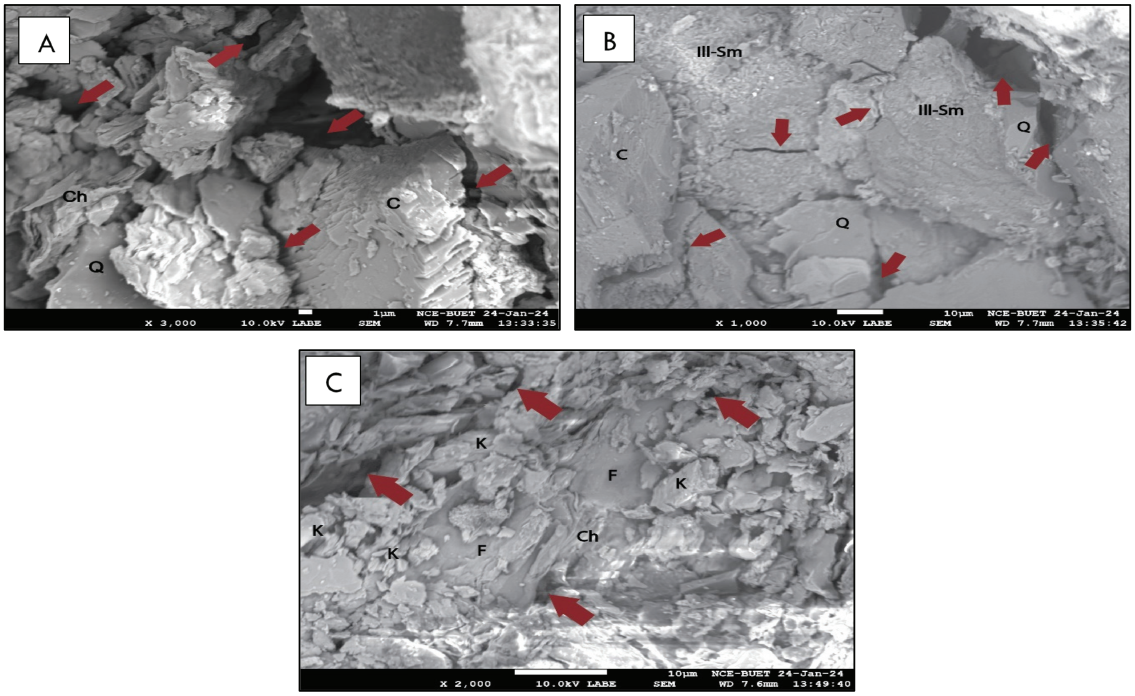

Figure 28: Scanning Electron Micrographs of Surma Group Sandstones Showing Quartz, Grain-Coating, Pore-Lining Chlorite, and Calcite Cementation (A); Quartz Grains Containing Microfractures, Illite-Smectite Mixed Layer Coating in the Grain Surfaces, and Calcite Cement (B); Detrital Feldspar, Chlorite Coating and Booklets of Kaolinite (C). Brown Arrows Show Connected Intergranular Pore Spaces, Intragranular Microfractures. The Minerals are Indicated as Q=Quartz, C= Calcite, Ch=Chlorite, F=Feldspar, K=Kaolinite, and Ill-Sm= Illite-Smectite

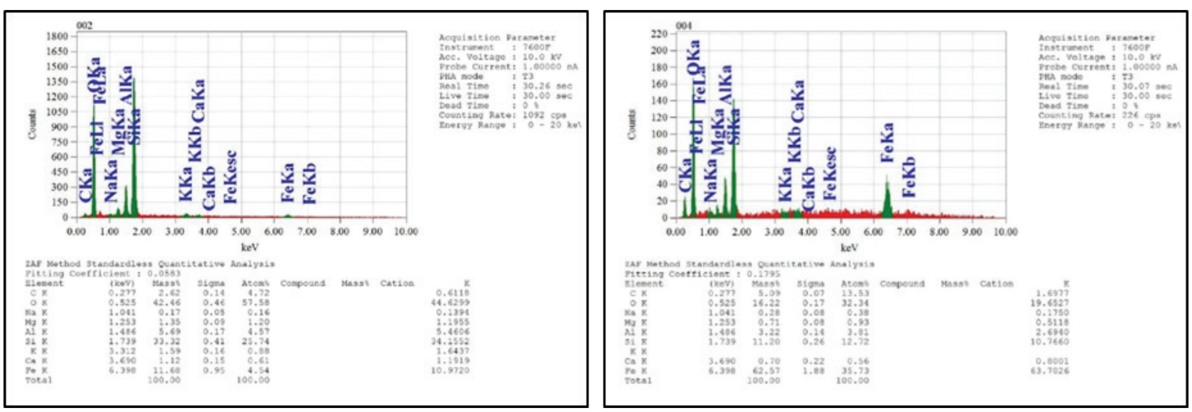

Figure 29: Atomic and Mass Percentage of the Analyzed Chemical Elements of EDS Spot Locations from Sample SP-4

Reservoir Quality of the Surma Group Sandstones

Reservoir properties of Surma group sandstone and prospects for hydrocarbon accumulation in the Eastern Fold Belt, especially in the Sitapahar structure, Kaptai, were analyzed using field data from four sections. Neogene Surma Group sandstone units were our main focus in this research, and sand-dominant facies associations in the investigated outcrops support the idea of a good reservoir unit.

Outcrops from the Shilchari Section, Boroichari Section, Lichubagan Section, and the Navy Road Section represent Surma Group deposits. They show higher sand content (arenaceous), which indicates the upper part of the Surma Group; thus, good reservoir quality can be assured. Lateral facies changes are observed as we move along the road-cut sections. The lithologic columns show sand-dominated, good-quality reservoir facies. Heterolithic tidal deposits indicate a fluvial-deltaic setting where a transition to Tipam sandstone can also be noticed.

The Bayzid Link Road section, the Labanakhya Chara-Sohosrodhara Waterfall Section, and the Chandranath-Microwave Roadcut section in Sitakund structure contain Surma Group sandstones. Massive sandstones with higher sand content in the Chandranath temple section of interbedded shales show good-quality reservoirs. The section along Microwave Road also contains a relatively lower number of shale interbeds, showing coarsening-upward and fining-upward cycles, and a single thin calcareous band, suggesting a suitable reservoir. The Labanakhya Chara-Sohosrodhara Waterfall Section contains many shale beds, nodular shales, and silty lenses in shales. Still, the upper part comprises a substantial number of sand beds with shale interbeds and alternating sand-shale sequences, suggesting moderate reservoir quality.

The reservoir quality of the Surma Group sandstone varies between the Sitapahar and Sitakund structures due to differences in depositional and diagenetic influences. In both areas, the depositional environment governs grain size, sorting, framework composition, and primary fabric, which in turn affect porosity and permeability. Thin-section analyses reveal that sandstones from Sitapahar are fine to medium-grained, sub-rounded to sub-angular, and moderately to well sorted, with porosity ranging from 7% to 21% and matrix content between 1% and 4%. Similarly, Sitakund sandstones exhibit fine to medium-grained textures, sub-angular to sub-rounded grains, and moderate to good sorting, with porosity between 5% and 20% and matrix content of 1% to 4%. Overall, both sites exhibit features indicative of good reservoir quality, though the Sitapahar samples display slightly higher porosity, suggesting a comparatively better reservoir potential.

Diagenetic processes exert a significant control on the reservoir quality of the Surma Group sandstones by modifying the original pore framework through both physical and chemical alterations during burial and post-burial evolution. The studied sandstones exhibit a wide range of diagenetic features that directly influence porosity, permeability, and pore-throat connectivity. Petrographic and microscopic observations indicate that compaction, cementation, dissolution, recrystallization, fracturing, and clay mineral transformations collectively governed the evolution of reservoir quality within the studied intervals.

Mechanical compaction is one of the major porosity-reducing processes in the studied sandstones. Due to increasing overburden pressure during burial, the sediments underwent grain rearrangement, tighter packing, and rotational adjustment of framework grains, resulting in a significant reduction of primary pore spaces. The sandstones are predominantly sublitharenites containing approximately 10–22% lithic fragments and abundant labile grains, making them particularly susceptible to compactional modification. Although a limited number of ductile grains are present, rigid framework grains helped locally preserve portions of the original pore system. Deformation features such as bent mica and chlorite flakes, plastically deformed shale fragments, and fractured feldspar grains indicate the influence of differential tectonic stress and burial-related compaction. Grain bending, fracturing, and localized microcracks contributed to the generation of secondary porosity in some intervals; however, overall compaction substantially reduced reservoir quality by increasing grain-to-grain contacts and decreasing pore connectivity.

Cementation also played a critical role in the destruction of porosity within the Surma Group sandstones. The studied samples display extensive quartz overgrowths formed through pressure solution, early poikilotopic calcite cementation, pore-filling calcite cement, chlorite coatings, localized kaolinite cementation, and late ferroan calcite precipitation. Among these, early poikilotopic calcite cementation is particularly effective in occluding pore spaces and, in some samples, reducing porosity and permeability almost completely. Quartz and calcite cements significantly restricted pore-throat connectivity, whereas late-stage ferroan calcite cement further degraded reservoir quality through extensive pore filling. Nevertheless, intervals characterized by limited cementation preserved appreciable primary porosity, indicating relatively favorable reservoir potential.

In contrast, dissolution processes contributed significantly to reservoir enhancement by developing secondary porosity. Dissolution of feldspar grains, lithic fragments, carbonate cements, and replacive calcite generated oversized, elongated, intragranular, and vuggy pores within the sandstones. Partial to complete dissolution of feldspar grains is common, and in some cases, more than 50% of feldspar grains exhibit dissolution features associated with acidic pore fluids. Dissolution of late ferroan calcite and replacive calcite is evidenced by floating and corroded grains, heterogeneous grain packing density, remnant cement stains adjacent to pores, and partially dissolved cement phases. Skeletal grains commonly display partial dissolution, whereas completely dissolved grains produce oversized secondary pores. Although minor quartz dissolution is observed locally, no evidence of leaching from the early poikilotopic calcite cement was identified. Overall, the dissolution and removal of unstable grains and pore-filling cements substantially enhanced effective porosity and improved reservoir quality in several intervals of the studied sandstones.

CONCLUSIONS

This study provides an integrated sedimentological, petrographic, diagenetic, and mineralogical characterization of the Neogene Surma Group sandstones exposed in the Sitapahar and Sitakund structures of the Eastern Fold Belt, Bengal Basin, Bangladesh. Using detailed outcrop logging, thin-section petrography, FE-SEM imaging, and EDS analyses, the study evaluates depositional environments, diagenetic evolution, pore-system development, and their implications for reservoir quality.

The major findings of the study are summarized as follows:

1. Facies associations indicate deposition within a tide-influenced deltaic to shallow-marine system comprising delta front–shoreface, delta plain, tidal-flat, prodeltaic, and tidal-influenced channel-fill environments.

2. The sandstones are predominantly medium- to fine-grained, moderately to well-sorted sublitharenites with low matrix content (<4%), indicating relatively mature and compositionally stable reservoir facies.

3. Mechanical compaction, pressure solution, quartz overgrowth, calcite cementation, and authigenic clay mineral formation significantly reduced primary porosity and pore-throat connectivity during burial diagenesis.

4. Dissolution of feldspar, lithic fragments, and carbonate cements generated secondary porosity in the form of moldic, elongated, oversized, and intragranular pores, locally improving reservoir quality.

5. FE-SEM observations reveal interconnected pore systems, while chlorite grain coatings locally preserved pore spaces by inhibiting extensive quartz cementation, despite partial permeability reduction caused by pore-lining clay minerals.

6. Comparative analyses suggest that the Sitapahar sandstones generally preserve slightly better reservoir quality than the Sitakund sandstones due to lower cementation intensity and enhanced pore preservation.

The Surma Group sandstones exhibit moderate to good hydrocarbon reservoir potential despite significant diagenetic overprinting. The results improve understanding of reservoir heterogeneity within the Eastern Fold Belt and provide insights into the controls governing sandstone reservoir evolution in the Bengal Basin.

Future studies should integrate core data, well-log interpretation, petrophysical measurements, geochemical analyses, and seismic data to better constrain burial history, fluid evolution, and basin-scale reservoir distribution.

ACKNOWLEDGEMENTS

The authors express their sincere gratitude to the University Grants Commission (UGC-DU 2023-24) for providing the necessary financial support to conduct the research. We are also grateful to the Department of Geology, University of Dhaka, for the provision of essential laboratory facilities. Furthermore, we extend our appreciation to the Bangladesh Petroleum Exploration and Production Company (BAPEX) and the Bangladesh University of Engineering and Technology (BUET), Department of Nanomaterials & Ceramic Engineering, for granting access to their respective laboratory facilities to perform the required analyses.

REFERENCES

Akter, M., Rahman, M. J. J., Ma, M., Hossain, D., Khanam, F., 2023. Depositional and diagenetic controls on reservoir quality of neogene Surma group from Srikail gas field, bengal basin, Bangladesh. Minerals 13(2), 283.

Akhter, S. H., 1979. *Structure, stratigraphy and sedimentology of the upper tertiary sediments of the central part of the Sitakund hill range, Chittagong, Bangladesh* (Unpublished M.Sc. thesis). Department of Geology, University of Dhaka, Bangladesh.

Alam, M., 1989. Geology and depositional history of Cenozoic sediments of the bengal basin of Bangladesh. *Palaeogeography, Palaeoclimatology, Palaeoecology 69*, 125–139. https://doi.org/10.1016/0031-0182(89)90159-4.

Alam, M., Alam, M. M., Curray, J. R., Chowdhury, M. L. R., Gani, M. R., 2003. An overview of the sedimentary geology of the bengal basin in relation to the regional tectonic framework and basin-fill history. *Sedimentary Geology 155*, 179–208.

Alam, M., Sikder, M., colleagues., 2003. Facies / sedimentology contributions on the Surma group (Miocene) - Bhuban and Bokabil formations. *(Commonly cited as "Alam et al., 2003" in Surma Group studies).*

Allison, M. A., Khan, S. R., Goodbred, S. L., Jr., Kuehl, S. A., 2003. Stratigraphic evolution of the late holocene Ganges–Brahmaputra lower delta plain. *Sedimentary Geology 155*(3–4), 317–342.

Allison, M. A., Kuehl, S. A., Martin, T. C., Hassan, A., 2003. Importance of flood-plain sedimentation for river sediment budgets and terrigenous input to the Ganges–Brahmaputra–Meghna delta. *Geology 31*, 189–192.

Banerjee, I., Sen, S., 1988. Modelling of tide-dominated sedimentary environments. *Sedimentary Geology 55*, 1–3.

Banerjee, M., Sen, A. K., 1988. Holocene transgression and deltaic progradation in the Ganges–Brahmaputra delta. *(Journal or conference; widely cited for transgressive phases and marine influence on facies).*

Bashar, K., Khan, A. A., 2008. Diagenesis and reservoir quality of Surma group sandstones, Sylhet Basin, Bangladesh. *Journal of the Geological Society of India 72*, 463–476.

Bashar, M. A., Khan, M. R., 2008. Diagenesis and reservoir quality of Neogene sandstones from the bengal basin, Bangladesh. *Journal of Asian Earth Sciences 31*(2), 105–118. https://doi.org/10.1016/j.jseaes.2007.07.006.

Chowdhury, S. R., Samanta, B. K., 2004. Diagenetic impact on reservoir quality of Surma group sandstones, bengal basin. *Indian Journal of Geosciences 58*, 41–52.

Chowdhury, S., Samanta, A., 2004. Diagenetic controls on porosity evolution of Miocene sandstones from the Surma basin, Bangladesh. *Sedimentary Geology 168*(3–4), 187–204. https://doi.org/10.1016/j.sedgeo.2004.03.005.

Curray, J. R., 1991a. Geological history of the bengal geosyncline. *Journal of the Association of Explor. Geophys, XII*, 209–219.

Dott, R. H., Jr., 1964. Wacke, greywacke and matrix—What approach to immature sandstone classification? Journal of Sedimentary Petrology 34(3), 625-632.

Evans, P., 1932. *The Tertiary succession in Assam*. Geology and Metallurgy Institute of India, Transactions in Mineralogy 30, 174–233.

Gazi, M. Y., Kabir, S. M. M., Imam, M. B., Rahman, A., Islam, M. A., 2017. Geochemistry of Neogene mudrocks from Sitakund anticline, bengal basin: Implications for provenance, weathering, tectonic setting and depositional environment. *Journal of Geoscience and Environment Protection 5*, 147–171. https://doi.org/10.4236/gep.2017.56015.

Goldstein, J. I., Newbury, D. E., Joy, D. C., Lyman, C. E., Echlin, P., Lifshin, E., Sawyer, L., Michael, J. R., 2003. *Scanning electron microscopy and X ray microanalysis* (3rd ed.). Springer. ISBN 978-0-306-47292-3.

Goodbred, S. L., Kuehl, S. A., 2000. The significance of large sediment supply, active tectonism, and eustasy on margin sequence development: Late quaternary stratigraphy and evolution of the Ganges–Brahmaputra delta. *Sedimentary Geology 133*, 227–248.

Hiller, K., Elahi, M., 1988. Structural growth and hydrocarbon entrapment in the Surma basin, Bangladesh (Northwest Indo-Burman Fold Belt) (SPE Paper 12398 MS). Society of Petroleum Engineers.

Holtrop, J. F., Keizer, J., 1970. Some aspects of the stratigraphy and correlation of the Surma basin wells, East Pakistan. *ECAFE Mineral Resources Development Series 36*, 143–154. Geological Society of India.

Hossain, N., Hossain, H. M., Sarder, M., Hasan, M., 2019. Origin and accumulation mechanism of gas condensate in Kailashtila gas field, Sylhet basin, Bangladesh. International Journal of Economic and Environmental Geology 10(1), 27–34.

Imam, B., 2013. *Energy resources of Bangladesh* (2nd ed.). University Grants Commission (UGC), Dhaka.

Imam, B., Hussain, M. M., 2002. Petrography and provenance of Neogene sandstones of the Surma group, bengal basin, Bangladesh. *Journal of Asian Earth Sciences 20*(6), 691–703. https://doi.org/10.1016/S1367-9120(01)00069-8.

Imam, B., Shaw, H. F., 1985. Diagenesis of neogene sandstones of the Surma group, bengal basin. *Sedimentary Geology 42*(3–4), 267–286. https://doi.org/10.1016/0037-0738(85)90028-7.

Islam, M. S., Habibullah, M., 2017. Clay mineral diagenesis and its impact on reservoir quality of Surma group sandstones, Bengal Basin, Bangladesh. *Arabian Journal of Geosciences 10*, 512. https://doi.org/10.1007/s12517-017-3295-3.

Islam, M. A., 2009. Diagenesis and reservoir quality of bhuban sandstones (Neogene), Titas gas field, bengal basin, Bangladesh. Journal of Asian Earth Sciences 35(1), 89-100.

Johnson, S. Y., Alam, A. M. N., 1991. Sedimentation and tectonics of the Sylhet trough, Bangladesh. *Geological Society of America Bulletin 103*, 1513–1527.

Khan, A. A., Chouhan, R. K. S., 1996. The crustal dynamics and the tectonic trends in the bengal basin. *Journal of Geodynamics 22*(3–4), 267–286.

Khan, A. A., Alam, M. M., Rahman, M. J., 1988. Structure and tectonics of the Chittagong-Tripura fold belt. *Tectonophysics 154*, 59–70.

Lohmann, G. P., 1995. The sedimentary geology and tectonic evolution of the bengal basin. In M. Alam (Ed.), *An overview of the sedimentary geology of the Bengal Basin* (pp. specific pages). Elsevier.

Morad, S., Ketzer, J. M., De Ros, L. F., 2000. Spatial and temporal distribution of diagenetic alterations in siliciclastic rocks: Implications for mass transfer in sedimentary basins. *Sedimentology 47*(1), 95–120. https://doi.org/10.1046/j.1365-3091.2000.00282.x.

Najman, Y., Bickle, M., BouDagher-Fadel, M., Carter, A., Garzanti, E., Paul, M., Wijbrans, J., Willett, E., Oliver, G., Parrish, R., Akhter, S. H., Allen, R., Ando, S., Chisty, E., Reisberg, L., Vezzoli, G., 2008. The Paleogene record of Himalayan erosion: bengal basin, Bangladesh. Earth and Planetary Science Letters 273(1–2), 1–14. https://doi.org/10.1016/j.epsl.2008.04.028.

Paul, P., Rahman, M., Md Sayem, A. S., 2026. Depositional and diagenetic controls on the reservoir quality of the Neogene Surma group in the Begumganj gas field, bengal basin (Bangladesh). Journal of Sedimentary Environments 11(1), 4.

Rahman, M.J.J., Mutti, M., Ma, M., Chen, G., Akhter, W., Akter, S., Hossain, M.S., Khan, M.R.A., 2022. Diagenetic controls on the reservoir quality of Neogene sandstones in the offshore area of the bengal basin, Bangladesh. Geological Journal 57(11), 4793-4814.

Rahman, M. J. J., & Worden, R. H. (2016). Diagenesis and its impact on the reservoir quality of Miocene sandstones (Surma Group) from the Bengal Basin, Bangladesh. Marine and Petroleum Geology, 77, 898-915.

Rahman, M. J. J., McCann, T., 2012. Diagenetic history of the Surma group sandstones (Miocene) in the Surma basin, Bangladesh. Journal of Asian Earth Sciences 45, 65-78.

Reimann, K. U., 1993. *Geology of Bangladesh*. Gebrüder Borntraeger.

Sayem, A. S. M., Rahman, M. J. J., Abdullah, R., Azim, K. R., 2022. Diagenetic history of the miocene Surma group sandstones from the eastern fold belt of the bengal basin. Journal of Asian Earth Sciences: X 7, 100098.

Sikder, A. M., 1998. Structural development of the eastern fold belt of the bengal basin, Bangladesh. *Sedimentary Geology*.

Sikder, A. M., Alam, M., 2003. 2D modelling of the tectonic evolution of the bengal basin. *Sedimentary Geology 155*, 209–226.

Uddin, A., Lundberg, N., 1998. Cenozoic history of the Himalayan-Bengal system: sedimentology and tectonics of the bengal basin. *Geological Society of America Bulletin 110*, 487–499.

Uddin, A., Lundberg, N., 2004. Miocene sedimentation and subsidence during continent–continent collision, bengal basin, Bangladesh. *Sedimentary Geology 164*(1–2), 131–146. https://doi.org/10.1016/j.sedgeo.2003.09.004.

Worden, R. H., Burley, S. D., 2003. Sandstone diagenesis: A key control on reservoir quality. In R. H. Worden & S. D. Burley (Eds.), *Sandstone Diagenesis* (pp. 3–44). Wiley-Blackwell.